



Review

Low-temperature ammonia decomposition catalysts for hydrogen generation



Shreya Mukherjee, Surya V. Devaguptapu, Anna Sviripa, Carl R.F. Lund, Gang Wu*

Department of Chemical and Biological Engineering, University at Buffalo, The State University of New York, Buffalo, NY 14260, United States

ARTICLE INFO

Keywords:

Ammonia
Decomposition
Low-temperature
Nonprecious metal catalysts
Hydrogen generation

ABSTRACT

Catalytic decomposition of ammonia with complete conversion for generating hydrogen at low temperature ($< 450^{\circ}\text{C}$) is getting much attention, as onsite hydrogen generation from ammonia bypasses the challenges of hydrogen storage and transportation. Ammonia is a carbon-free hydrogen carrier with a reasonably good volumetric and gravimetric energy density that has available technology for efficient storage and transportation. The state-of-the-art catalysts for decomposition of ammonia are ruthenium doped with potassium, barium and cesium and supported on various oxides and carbon supports; these catalysts are still not sufficiently active for low temperature NH_3 decomposition, and, more importantly, will not be economically viable for large-scale applications. This review provides a comprehensive consideration of recent development of various types of nonprecious transition metal catalysts. Proposed mechanisms of ammonia decomposition on various transition metals are examined, and theoretical bases for the design of future catalysts are presented, including the role of electronic promoters and supports. Among studied catalyst formulations, this review emphasizes transition metal nitride-lithium imide composites where a synergy offers great promise for the efficient decomposition of ammonia at low temperatures. Development of such catalysts will make hydrogen storage, transportation, and generation from ammonia a feasible technology for fuel cells and other energy applications.

1. Introduction

Hydrogen, the simplest and most plentiful element in the universe, can be used in fuel cells to generate electricity and drive motor vehicles without CO_x and NO_x emission, besides providing backup power and grid stabilization applications [1,2]. Its enthalpy of combustion is 142 MJ kg^{-1} , much greater than most other fuels, but when continuous delivery, e.g. via pipeline, is not practical or possible, hydrogen either must be stored or generated at the point of use. Its volatility and low volumetric energy density makes the storage and transportation of hydrogen, or a reagent from which it can be generated, a grand challenge. In early 2001, Schlapbach et al. published a review on hydrogen storage materials for mobile applications and included the major advantages and limitations of hydrogen as a fuel. Though hydrogen is the most abundant element on earth, it is available mostly in the form of water or as gaseous hydrocarbons. Thus, a lot of energy from fossil fuels is spent in deriving hydrogen using steam reforming, water splitting etc. To run 400 km, an hydrogen fuel cell electric car would require to store 4 kg of hydrogen at 200 bar [2]. The Toyota Mirai in 2016, a newly commercialized fuel cell car with a cruising range of 312 miles (502 km approx.) uses 2 carbon fiber high pressure tanks: one at the rear (62.4 L)

and the other in the front (60.0 L) [3]. However, the energy consumed in H_2 compression has to be considered as well. Thus, technology for eco-friendly hydrogen carriers to make onsite hydrogen generation is highly demanded [4].

Hydrocarbon fuels like natural gas, gasoline, methanol etc. can be thought of as a form of stored hydrogen, but most commonly these fuels are burned directly and not converted to hydrogen. The environmental consequences of burning these fuels directly motivate the search for alternative, carbon-free means of generating hydrogen [5–8] in an eco-friendly way [9–11]. Fig. 1 [12] compares the mass and density of various materials that can be stored for conversion to hydrogen. In solid form, metal amine salts are much lighter than metal hydrides storing an equal amount of hydrogen. As the figure shows, $\text{Ca}(\text{NH}_3)_8\text{Cl}_2$ and $\text{Mg}(\text{NH}_3)_6\text{Cl}_2$ take 102 kg and 109 kg weight, respectively, to store 10 kg of hydrogen compared to 390 kg of Mg_2NiH_4 and 730 kg of LaNi_5H_6 , and, at the same time, their density is greater so they occupy less volume.

1.1. Development of storage vectors for hydrogen

Hydrogen and reagents to generate hydrogen are energy vectors, which allow energy to be stored, transported and converted to another

* Corresponding author.

E-mail address: gangwu@buffalo.edu (G. Wu).

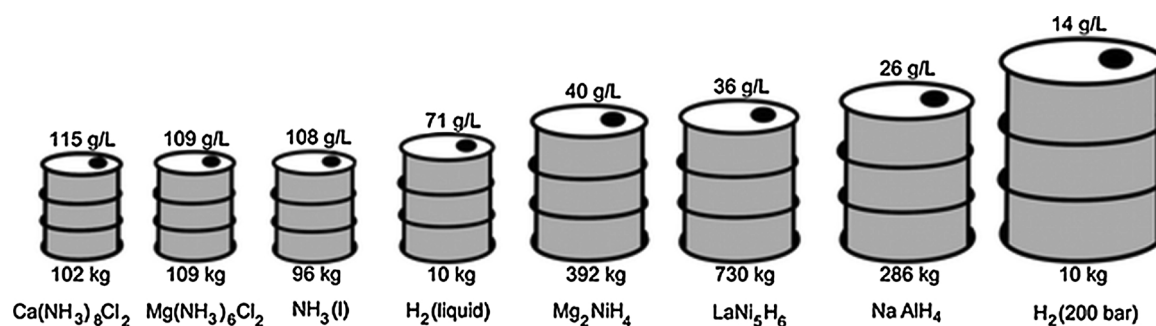


Fig. 1. Comparison of equivalent mass and volume of 10 kg of hydrogen stored by 8 different reversible methods based on reversible gravimetric and volumetric densities reported in the literature. The volume and weight of the container is neglected.

With permission to reprint from Ref [12], Copyright 2008, Royal Society of Chemistry.

form such as electricity. As noted, an alternative to direct combustion of hydrocarbon fuels is to use them as hydrogen vectors, converting them to hydrogen at the point of use. One of the first such vectors investigated for hydrogen generation at onsite storage was methanol [13]; it has a good lower heating value (638 kJ/mole) and a high hydrogen volumetric content of 87 kg/m³ (12.5% on a mass basis). However, on-vehicle conversion of methanol to hydrogen yields CO_x, and since on-vehicle capture is infeasible, undesirable CO_x emissions result, just as if the methanol had been burned directly.

Several complex metal hydrides like NaAlH₄, LiAlH₄, Mg(BH₄)₂, and amide/imides systems have been developed for hydrogen storage. They eliminate CO_x emissions, but they have not succeeded in meeting the U.S. Department of Energy targets for reversible hydrogen storage capacity for on-board hydrogen storage systems [12,14]. Substantial research on hydrogen adsorption in carbon nanostructures and metal-organic frameworks, MOFs, also has been conducted, but these systems lack efficient reversibility [15]. More recently, metal amine salts, which can store 9.1% hydrogen by weight, have been examined [16,17]. Metal amine salts have a higher density of stored hydrogen than hydrides but these complexes thermally decompose to give ammonia and require an ammonia decomposition catalyst to evolve hydrogen [16]. If ammonia decomposition catalyst has to be used to generate hydrogen from metal amine salts, it would be rather beneficial to decompose ammonia at low temperatures for hydrogen generation.

Over the last decade, ammonia emerged as an efficient hydrogen carrier due to its high volumetric energy density (108 kg-H₂/m³ NH₃ at 20 °C and 8.6 bar) and gravimetric energy density (17.8 wt.%), combined with its ease of storage and transportation [18–20]. Ammonia is also a high volume commercial chemical, with global production of 176 million metric tons in 2014 [21]. Table 1 compares conventional fuels to ammonia with respect to heating value, energy density, specific volumetric cost, and specific energetic cost. [22]. Though the heating value of gasoline is much higher than ammonia, the specific energy cost for ammonia is lower. Compared to other fuels like liquefied petroleum gas (LPG), methanol, and metal hydrides, ammonia has a lower specific energy cost.

Table 1

Comparison of fuels for hydrogen storage.

With permission to reprint from Ref [12], Copyright 2008, Journal of Power sources [22].

Fuel/storage	P (bar)	Density (kg m ⁻³)	HHV, (MJ kg ⁻¹)	Energy Density, (GJ m ⁻³)	Specific volumetric cost, (\$ m ⁻³)	Specific energetic cost, (\$ GJ ⁻¹)
Gasoline C ₈ H ₁₈ /liquid tank	1	736	46.7	34.4	1000	29.1
CNG CH ₄ /Integrated Storage system	250	188	55.5	10.4	400	38.3
LPG	14	288	48.9	19	542	28.5
Methanol	1	749	15.2	11.4	693	60.9
Hydrogen/Metal hydrides	14	25	142	3.5	125	35.2
Ammonia/Pressurised tank	10	603	22.5	13.5	181	13.3
Ammonia/Metal amines	1	610	17.1	10.4	183	17.5

Another attractive aspect of ammonia as a hydrogen carrier is that the ammonia decomposition reaction is more economical than methanol reforming [23,24]. In addition, for fuel cell applications, the hydrogen generated via ammonia decomposition has scant impurities [2,25] compared to hydrogen generated from hydrocarbons. The suitability of ammonia as a fuel for mobile and remote applications has already been explored [12,20,22,24,26–30]. It has the potential to be the best carbon-free source of hydrogen for fuel cell applications, if nonprecious catalysts can be developed to make the complete decomposition reaction (100% conversion) viable at lower operating temperatures (< 450 °C). PEM fuel cells are sensitive to ammonia of the order of 1 ppm. There are several catalysts for the ammonia decomposition reaction but they attain complete conversion only at temperatures over 650 °C. For solid oxide fuel cells (SOFCs), ammonia can be directly fed and complete conversion is not essential [31]. They operate at temperatures between 500 and 800 °C. Such a high temperature will make the onsite hydrogen storage application less energy efficient. Thus, development of catalysts to attain complete conversion at low temperature is critically important to make onsite hydrogen generation from ammonia a feasible technology.

1.2. A brief history of ammonia decomposition catalysts

As noted, efficient generation of hydrogen from ammonia-based reagents is critical to their utilization as hydrogen energy vectors. Synthesis and decomposition of ammonia are one reaction occurring in opposite directions, and they often share a rate-determining step: the adsorption/desorption of dinitrogen [32]. Nonetheless, the best catalyst for ammonia synthesis does not prove to be the best catalyst for the decomposition reaction [18], because the reaction conditions are different. Specifically, ammonia decomposition occurs at high partial pressures of ammonia, and as a consequence, the species present on the catalyst surface and their relative concentrations during ammonia decomposition are very different from those during ammonia synthesis. In addition, the rate limiting step can vary, depending on the nature of the catalyst, the geometry of the active sites [33], the nature of support and

promoters [34–37] etc. In 1904, Perman and Atkinson reported that decomposition of ammonia cannot be considered complete at temperature below 1100 °C. However, they also mentioned that the extent of decomposition is related to the nature of the surface that ammonia is in contact with, *i.e.* catalysts [38].

Research on ammonia decomposition catalysis has gained momentum in the last two decades [[36],39–45], even though it often has been studied from the perspective of improving understanding of ammonia synthesis [46,47]. Platinum [48], palladium, rhodium, and ruthenium [49] were the first elements to be investigated as ammonia decomposition catalysts, besides iron [50,51] that were known catalyze ammonia synthesis. Ganley et al. [52] expanded the number of metals studied for their catalytic activity for ammonia decomposition and reported their activity in a decreasing order to be Ru > Ni > Rh > Co > Ir > Fe > Pt > Cr > Pd > Cu > Te, Se, Pb [52]. Although ruthenium shows the best activity among these metals, its activity at lower temperatures is not adequate. The conversion for Ru supported on carbon nanotube (CNT) at 450 °C is less than 50% [36]. In attempts to address this shortcoming, the roles of catalyst formulation, catalyst synthesis, supports and promoters on ruthenium have been investigated and are highlighted in Section 3.1 of this review. Ru supported on MgO or CNT and modified with alkali promoters like KNO_3 has improved activity at temperature below 500 °C. Some studies were also aimed at stabilizing small Ru nanoparticles, for instance by embedding them in stable and porous oxides, and preventing fast deactivation by sintering [53]. While these studies have resulted in better catalysts, [34,54–56], large scale use of ruthenium may not be feasible due to its high cost and scarcity [57]. Consequently, derivatives of other transition metals, like Ni [58–60] Fe [61,62], and Co [63,64] on a variety of supports have also been explored extensively for ammonia decomposition [[36],35,65].

Several previous reviews have considered hydrogen vectors especially ammonia as a hydrogen storage vector [2]. Klerke et al. [12] emphasized various challenges and opportunities of ammonia as a fuel. Xu et al. [66] focused on Ru catalysts for ammonia decomposition and examined the role of various supports and promoters through 2004. Later, Schueth et al. [29] provided details of the treatment of gases after ammonia decomposition at a fueling station; their focus was on catalysts developed before 2011. They suggested that even though complete conversion of ammonia does not occur, in fuel cell applications unconverted ammonia could be adsorbed using resin or zeolite, so that it does not poison the fuel cell anode. They also pointed out that onboard regeneration of the zeolite adsorbent is possible at temperatures around 327 °C, which would be close to the temperature of ammonia decomposition. Hence, heat integration in a fueling station would not be an issue. Supports and promoters used for nonprecious metal catalysts such as iron, cobalt, nickel, and some bimetallic catalysts were reviewed by Bell et al. [67].

In this review, in the following section, by examining single-component materials that have been reported to catalyze the decomposition of ammonia. The reaction mechanism and kinetics and the low-temperature activity of the catalysts are emphasized. That review reveals that to date, no single-component catalysts with high activity at low temperatures have been identified. In section 3, we review catalyst development efforts seeking to improve ammonia decomposition performance. Reported use and effects of supports and promoters upon the performance of single component catalysts as well as formulation of multicomponent catalysts are discussed. By paying particular attention to recently developed low-temperature decomposition catalysts based on amides, imides, nitride-imide composites etc., and comparing the mechanism and kinetics for them to the more traditional catalysts, we have attempted to provide a perspective for the design of high-performance nonprecious metal catalysts using advanced supports and promoters.

2. Mechanism and kinetics of ammonia decomposition

Though ruthenium is too expensive to be the future catalyst for ammonia decomposition at low temperature, it has been studied extensively, as have several other metals. Investigation of the mechanism of the reaction kinetics provides a rational basis for understanding the effects of catalyst formulation and synthesis, promoters, and supports. Further, relating the effects of those aspects of catalyst modification to the mechanism of the reaction provides insight for the future design of advanced catalysts.

2.1. Metal catalysts

In one of the first systematic studies on the mechanism of ammonia decomposition over iron in 1942, Brauner and Love [51] indicated that the slowest step in the decomposition is the desorption of nitrogen. However, the rate of ammonia decomposition over the iron-based catalysts shows a very complex dependence on the partial pressures of hydrogen and ammonia, as well as on the temperature. For unsupported ruthenium, the kinetics of the reaction limit conversions at practical conditions to only 32.5% [68]. Thus, in addition to catalysis, reaction engineering of ammonia decomposition reactors, especially for low-temperature, high conversion operation, is an active field of study [69–75].

Over metals, the decomposition of ammonia occurs in a stepwise sequence of dehydrogenation reactions. The reaction sequence begins with adsorption of ammonia on the metal surface. Generally, nitrogen adsorption is thought to be rate-limiting in ammonia synthesis while the rate determining step for ammonia decomposition varies. On precious metals like Ru, Rh, Ir, Pt, or Pd, NH cleavage is the rate-determining step, while, for nonprecious metals like Fe, Co, or Ni, N_2 desorption is the rate-determining step [18,32]. The kinetic models on precious and non-precious elements are also discussed at the end of this section. A recent temporal analysis of products (TAP) study on Ru revealed that the recombination of nitrogen atoms is the slowest step during ammonia decomposition [76]. In 1984, Egawa et al. [33] studied different crystal planes of Ru and found that the rate of hydrogen formation on Ru (1110) is one order of magnitude higher than on Ru (0001). It was suggested that the active sites consisted of an arrangement of three Ru atoms in the surface layer and two additional Ru atoms in a sub-surface layer [77]. According to density functional theory (DFT) calculations, these so-called B-5 sites exhibit an adsorption energy that facilitates desorption of nitrogen molecules. The importance of metal coordination was further supported by results obtained by Mortensen et al. [78], who studied the dynamics of decomposition by varying the incident energy of ammonia striking the surface by using molecular beam techniques.

Duan et al. [79] used DFT and surface models of Fe(110), Co(111) and Ni(111) to study the mechanism of ammonia decomposition. As shown in Fig. 2 [79], the initial dehydrogenation leads to on-top adsorption of ammonia for all three metals, which is followed by formation of NH_2^* and H. Then NH_2^* moves to a bridge site and dissociates to NH and H. Next, the NH moves from the bridge site to an interstitial site where the final dehydrogenation occurs. The H atom from the second dehydrogenation stays at a bridge site for Fe, but moves to an interstitial site for Ni and Co, due to differences in binding energy. The authors noted that the *d*-band centre of Fe(110) is the nearest to the Fermi level, and the adsorption energy for the adsorbed species is therefore the highest [79]. For all three catalysts, N is present at the interstitial site after the dehydrogenation steps, and the energy barrier for associative desorption of N is critical. Therefore, nitrogen desorption is the rate limiting step. For Fe, the magnitude of that barrier results in a high coverage of N blocking the Fe catalytic sites. Hence, Fe is considered to be relatively poor as a catalyst for ammonia decomposition when compared to Ni and Co [48,52,79].

Ganley et al. [52] calculated the rate of nitrogen desorption using

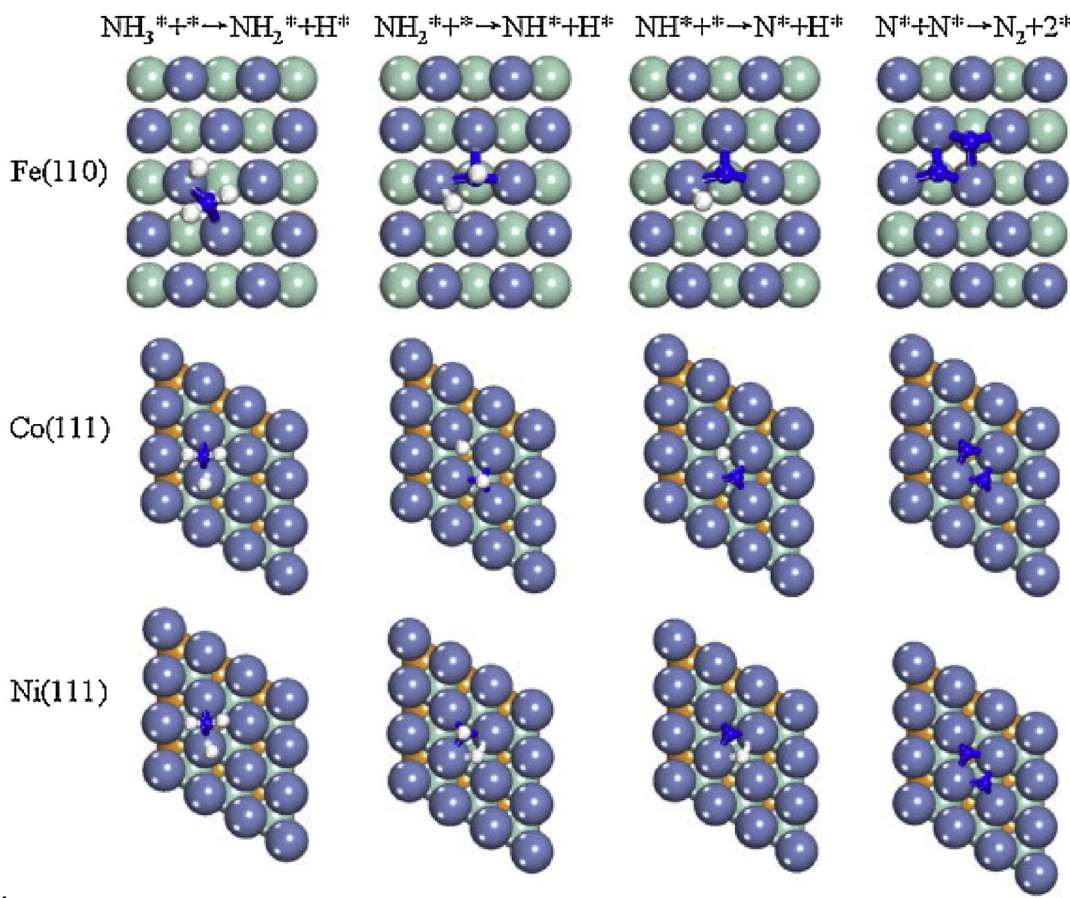


Fig. 2. Top view of the transition states of the NH_3 stepwise dehydrogenation reactions and the associative desorption of N on Fe(110), Co(111), and Ni(111) surfaces. With permission to reprint from Ref [79], Copyright 2012, Elsevier.

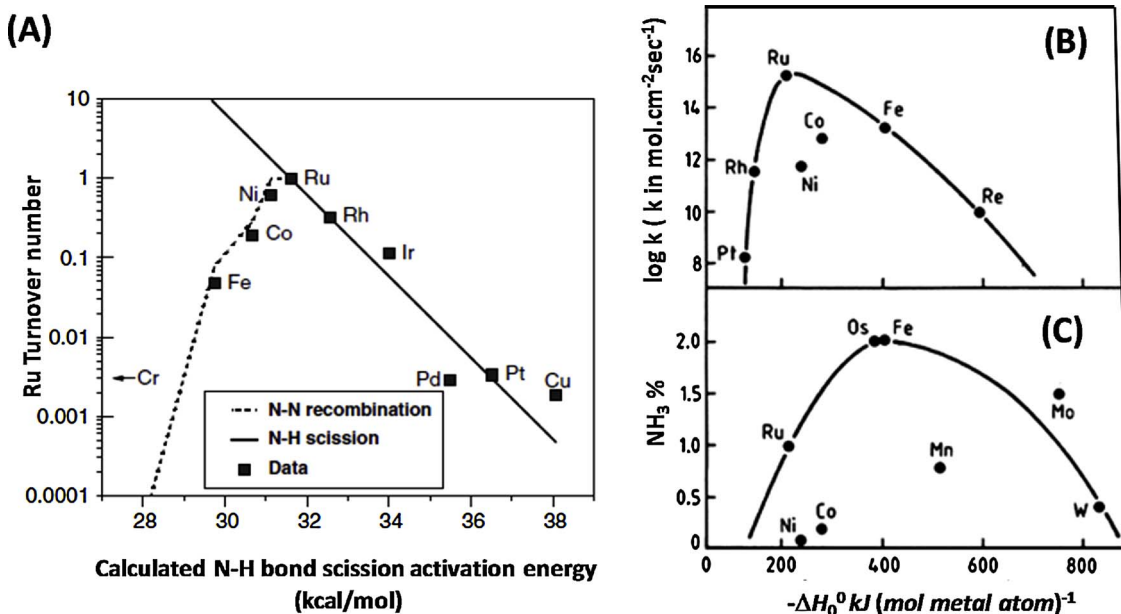


Fig. 3. (A) Variation of the TOF of different transition metals with activation energy for N–H bond scission estimated using Blowers-Masel correlation. Opposing trends are observed because the rate-determined step is different for these elements. With permission to reprint from Ref [52], Copyright 2004, Elsevier. (B) Variation of the rate constant for ammonia decomposition as a function of the enthalpy of reaction. (C) Variation of the capacity of ammonia synthesis over metals as a function of the enthalpy of reaction. With permission to reprint from Ref [29], Copyright 2012, Royal Society of Chemistry.

nitrogen bond energies for several metals. They found that the decomposition turnover frequency (TOF) increases with the activation energy for N–H bond cleavage for Ni, Co, Fe, and Cr, while it decreases

for Rh, Pt, Ir, Cu, and Pd leading to the volcano plot shown in Fig. 3(A) [52]. Their work indicates that for the precious metals, N–H cleavage is the rate determining step, whereas for ferrous metals, nitrogen

desorption is rate determining. Fig. 3(B) [29] is a volcano plot that shows variation in metal activity as a function of enthalpy for ammonia decomposition, whereas Fig. 3(C) [29] shows the same for ammonia synthesis. Ru is found at the peak of the volcano plot for ammonia decomposition, while iron represents the maximum for ammonia synthesis.

Given the differences in rate for different crystallographic planes of a single metal and the differences in rate-determining step between metals, it is not surprising that the reaction kinetics vary from one study to the next. Tsai et al. reported the temperature dependence of the rate on Ru (0001). Below 377 °C nitrogen desorption is rate limiting, whereas above 477 °C, it is N–H cleavage [80]. Thus, for low temperature decomposition, where nitrogen desorption is the slowest step, the kinetics are dependent on the partial pressures of hydrogen and ammonia, which establish the equilibrium nitrogen surface concentration. Increased hydrogen partial pressure decreases the concentration of surface nitrogen and thereby inhibits the reaction [33]. At high temperature, N–H cleavage becomes rate limiting and the kinetics are dependent on the partial pressure of ammonia which establishes the surface concentration of adsorbed ammonia. Pyrez et al. [81] studied K promoted Ru catalyst using different NH₃ concentrations and concluded that conversion decreases with increasing NH₃ concentration. Similarly, Cheleppa et al. found that over Ni-Pt/Al₂O₃, the decomposition kinetics of pure ammonia are different from those of diluted ammonia [56,82].

On iron and some other transition metals, for which the Temkin-Pyzhev mechanism applies, the rate of decomposition (Eq. (1)) is affected by the hydrogen pressure. This mechanism occurs at lower temperatures, and it is assumed that the nitrogen desorption rate is retarded or inhibited by hydrogen accumulated on the surface, thus reducing the overall decomposition rate [83].

$$r = k \left(\frac{P_{NH_3}}{P_{H_2}} \right)^\alpha \quad (1)$$

While studying mechanism of decomposition of ammonia on tungsten metal, Tamaru et al. [83] used direct adsorption measurements to link the amount and structure of adsorbed species to the reactivity. The rate of the reaction was found to be a function of the partial pressure of ammonia as shown in Eq. (2)

$$r = \frac{kP_{NH_3}}{1 + kP_{NH_3}} \quad (2)$$

Thus, the reaction rate is zero order at higher pressures of ammonia and first order at lower pressures of ammonia. At higher temperature, on metals like tungsten, molybdenum, and platinum, the decomposition rate increases with the partial pressure of ammonia. The adsorption in this case is favored at terrace sites [33].

The first systematic study on precious metals by Papaolymerou and Bontozoglou [84] used polycrystalline wires or foils of Pd, Ir, Pt, and Rh. Specifically, they compared ammonia decomposition on Pd and Ir wires to that on Pt and Rh. On the basis of those experiments, they proposed a Langmuir-Hinshelwood kinetic model where the rates at high temperature for each of the metals are first order in reactant pressure whereas at low temperature the reaction becomes pressure independent [84]. Goodman and co-workers [85] found that the catalytic activity of ammonia decomposition on Ru is much higher than that on Ir at equal loadings of the precious metals and with pure NH₃ as the reactant [56].

2.2. Nitride and carbide catalysts

Carbides and nitrides of Fe, Co, Ni, Ti, V, Mn, and Cr, can also act as catalysts, showing comparable activity to precious metals [86,87]. Boudart and Levy showed that tungsten carbides exhibit platinum-like catalytic properties for various reactions [88]. Zheng et al. demonstrated good catalytic activity of molybdenum carbide for ammonia

decomposition [89]. In the case of vanadium, it has been inferred that the 3d states of vanadium interact strongly with the 2p states of carbon, thereby changing the electron density of states at the fermi level and imparting an electronic structure similar to that of the precious metals [90]. Generally, the carbon and nitrogen in the metal carbides and metal nitride occupy the interstitial sites between the large metal atoms and therefore alter the electronic properties of the surface. This reduces the activation energy for decomposition of ammonia on the surface of nitrides and carbides. It was proposed that ammonia decomposition over transition metals nitrides proceeds through successive dehydrogenation and nitrogen desorption like on Fe (110) and Ni (111). For vanadium nitride, there is no partial pressure dependence on ammonia or hydrogen [91]. The mechanism is similar to that on tungsten with nitrogen desorption being the rate-determining step [92].

Decomposition of ammonia over molybdenum carbide in the 450–600 °C temperature range has an activation energy of 89 kJ/mole, similar to 2 wt.% Ru on various carbon supports. Choi was among the first to study the relationship between the structure of vanadium carbide and its activity for ammonia decomposition [90]. It was one of the first studies to explore metals other than Fe, Ni and Ru. Vanadium carbide catalysts also showed similar catalytic activity to Pt and other transition metal catalysts, in agreement with the theoretical calculations of Boudart and Levy [88,93,94]. They further stated that metallic vanadium films were not very active in ammonia decomposition but became activated after bulk nitridation. Doping with carbon and nitrogen changes the electrical and structural properties differently. Choi et al. studied vanadium nitride as well, and reported the activity to be less than that of the carbide, which is less than the activity of Mo₂C but higher than Pt. Thus, nitridation and carburization have induced catalytic activity in the original metals.

Another interesting class of materials derived from the usage of nitrides are oxy-nitrides. Zirconium oxy-nitrides have been found to be catalytically active for ammonia decomposition [95–97]. They are intrinsically reactive towards nitrogen and cannot be easily reduced. Fig. 4(A) shows the variation of the catalytic activity with particle sizes [95]. There is a sudden onset of catalytic activity of ZrON at ~550 °C, as shown in Fig. 4(B). Based on the structure sensitivity of ammonia decomposition, the sudden onset in activity is suggested to be due to rapid structural phase changes in the catalyst from the initial β phase to β' ZrON [95].

2.3. Mechanism of decomposition on metal amides/imides

Another alternative to metals is developing and using alkali metal amides as catalysts. It was first observed in 1894 by Titherley that an interesting result is obtained on heating sodium amide (NaNH₂) to dull redness in flowing ammonia. As a result, ammonia is continuously decomposed into its elements [98]. Surprisingly no additional study of NaNH₂ as catalyst is reported until 2014, when David et al. [25] conducted a study of ammonia decomposition using sodamide as the catalyst. They reported a conversion of 99.2% with 0.5 g of NaNH₂ and 60 sccm of NH₃ flow at 530 °C. The origin of the produced hydrogen, whether from the decomposition of ammonia or from the amide itself, was debated. Na and NaNH₂ exist in equilibrium at an intermediate temperature of around 400 °C. The authors hypothesized that equilibrium is established between sodium metal and sodium amide, and decomposition of ammonia is favored in the process. The two cyclic reactions are shown in Eqs. (3) and (4): sodium amide decomposes to form sodium metal, and sodium metal reacts with ammonia to give back sodium amide. If decomposition of sodium amide and ammonia were occurring simultaneously, the decomposition of ammonia would not be stoichiometric, however it was observed to be stoichiometric by Rietveld analysis.



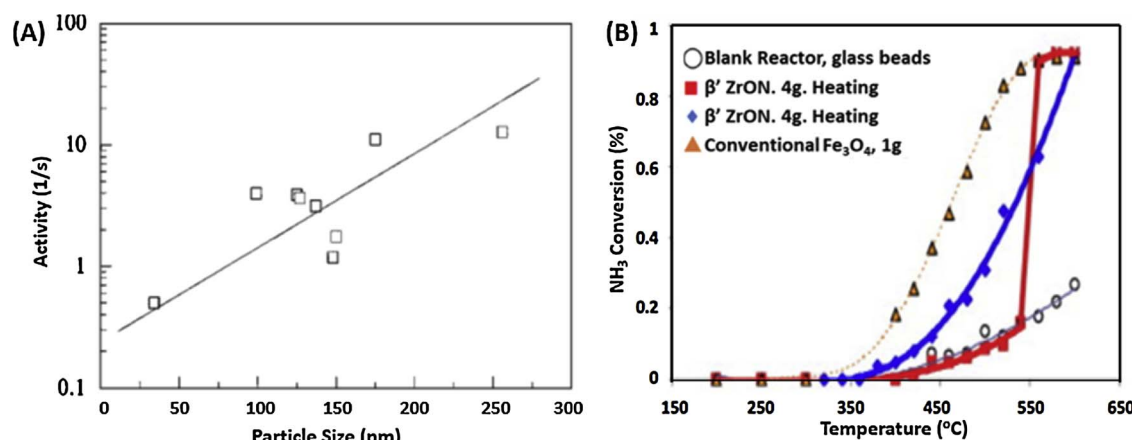
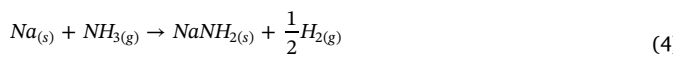


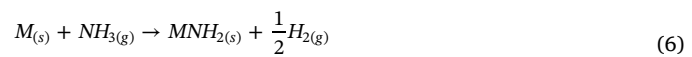
Fig. 4. (A) Variation of ammonia decomposition reaction catalytic activity with particle size of catalyst vanadium carbide. (B) Conversion of ammonia under steady state conditions as a function of temperature over a conventional iron oxide based catalyst (open triangles) ZrON during heating (black squares) and cooling (black diamond) using a feed of 50 mL STP/min He containing 4100 ppm NH₃. A blank reactor experiment with glass beads (open cycles) is included (shown in circles).

With permission to reprint from Ref [95], Copyright 2007, Elsevier.



During reaction, Na/NaNH₂ exists as an aerosol within the reactor. When they tested the samples post reaction by neutron powder diffraction, it was confirmed that NaNH₂ was a major crystalline component of the sample, which would not be the case if it had decomposed. The authors also mention that for the equilibrium reaction between sodium and amide, the equilibrium shifts towards formation of sodium metal at high temperature. Similarly, at low temperature, it should be directed towards formation of sodium amide. Since, sodium amide has a very low melting point (210 °C) and a boiling point of (400 °C) we suspect that sodium amide may have decomposed. However, when the reactor is cooled down and when the post reaction samples were analyzed, sodium amide may have formed again. Since, stability of NaNH₂ is a concern, they added baffles in the reactor. The addition of baffle enhanced the containment and increased the conversion efficiency. At a flow rate of 20 sccm, the conversion efficiency was 99.98% for 0.5 g of catalytic loading at 500 °C. However, the conversion efficiency is decreased with an increase in flow rates. The efficiency decreased to 96.5% at 50 sccm and 63.3% at 500 sccm. Decreased conversion with flow rates was also observed in other studies and can be improved by optimizing reactor design.

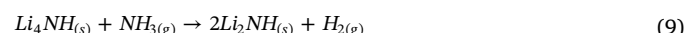
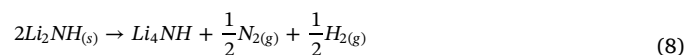
Following this promising work of ammonia decomposition with 99.9% conversion at 500 °C. Wood et al. [99] conducted an isotopic study of the decomposition of ammonia on sodium amide to predict the rate determining step and confirmed that the hydrogen evolution is from the decomposition of ammonia on the surface of sodium amide and not from the decomposition of sodium amide itself. When NH₃ was replaced with ND₃, it was found that the rate-limiting step involves a bond, which contains H/D. Since this could also involve the decomposition of NaNH₂, the same test was repeated in Ar instead of NH₃ or ND₃. However, in Ar, no kinetic isotope effect was observed. This proved that the scission of NH or ND was from NH₃ or ND₃ and not from NaNH₂. Thus, they confirmed that the equilibrium reactions between sodium metal and sodium amide as shown in Eqs. (3) and (4) are very important in the kinetics of ammonia decomposition. They also confirmed that N₂ formation is not the rate-limiting step in this system. Through this study, they also established that the role of the amide is not that of a mere promoter; it can act as a catalyst all by itself. The generalised mechanism of decomposition of ammonia on sodium based metal (like potassium and rubidium) was further given as in Eqs. (5) and (6).



The other significant amide studied for ammonia decomposition is lithium amide, which has been widely investigated for hydrogen storage [100–105]. It does not follow the same mechanism of decomposition as sodium amide. It decomposes thermally to form lithium imide and ammonia [106]. The investigation of various solid state hydrogen storage materials opened the path for analysis of lithium-nitrogen-hydrogen systems [107–110], in which hydrogen is stored in lithium nitride as lithium amide and lithium imide [111]. Miwa et al. summarized that the [NH₂][−] anion in lithium amide forms strong internal bonds with a covalent character [112]. Makepeace et al. [106] achieved 90.7% conversion at 458 °C when starting with lithium amide as the catalyst, but it decomposed into lithium imide during the reaction. Lithium amide melts at 360 °C and on further heating forms solid lithium imide whose decomposition temperature is around 600 °C as shown in Eq. (7).



Zhang et al. studied the kinetics of lithium imide decomposition and reported that lithium imide decomposes to form another complex Li₄NH, which further decomposes to Li metal, N₂ and H₂ [113]. Thus, decomposition of ammonia on lithium imide or lithium amide is non stoichiometric [106]. An isotopic study was further confirmed that decomposition of ammonia is associated with the decomposition of lithium imide to form the complex Li₄NH, which reacts with NH₃ again to produce Li₂NH, N₂, and H₂ as shown in Eqs. (8) and (9) [114].



Temperature dependence of ammonia conversion on both sodium amide and lithium amide is shown in Fig. 5(A) [106]. Though lithium amide decomposes to lithium imide, lithium imide alone would react with ammonia to give back lithium amide accompanying with generation of H₂ and N₂. Thus, at any given temperature ammonia decomposition occurs on nonstoichiometric lithium imide [106]. Further, mixed metal imides were tested as catalysts for ammonia decomposition and Fig. 5 (B) presents conversion profiles for lithium calcium imide and lithium magnesium imide [115], but not showing enhanced activity relative to individual lithium amide.

Thus, the mechanism of decomposition on precious metals like Ru, Pt, and Rh are different than those on nonprecious metals like Fe, Co, and Ni. However, the difference is the rate determining step. For

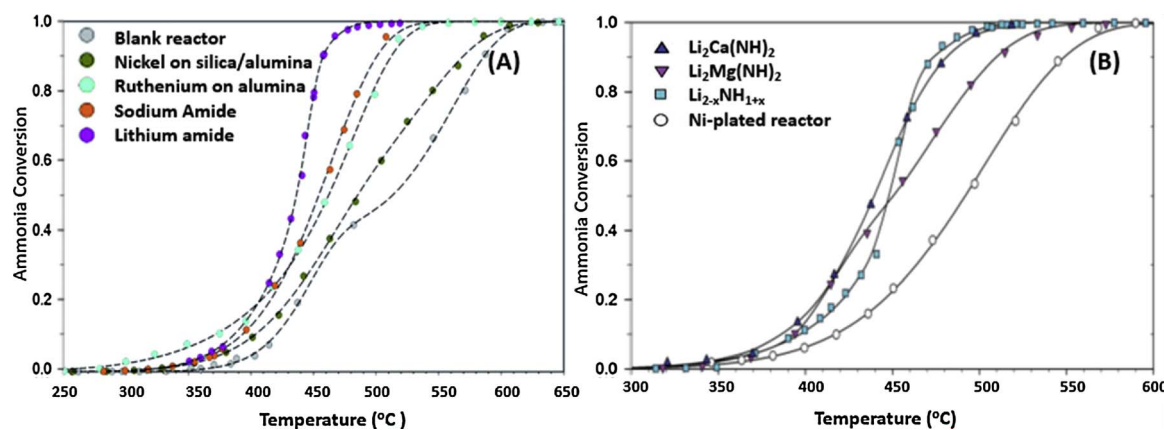


Fig. 5. (A) Comparison of ammonia conversion profile over metal amides and traditional metal catalyst in a stainless steel reactor using 0.5 g of catalyst with ammonia fed at 60 sccm. With permission to reprint from Ref [106], Copyright 2015, Royal Society of Chemistry. (B) Conversion of ammonia as a function of temperature on binary metal amides. $\text{Li}_2\text{Ca}(\text{NH})_2$ and $\text{Li}_2\text{Mg}(\text{NH})_2$ show considerable conversion at 500 °C and lower.

With permission to reprint from Ref [115], Copyright 2016, Royal Society of Chemistry.

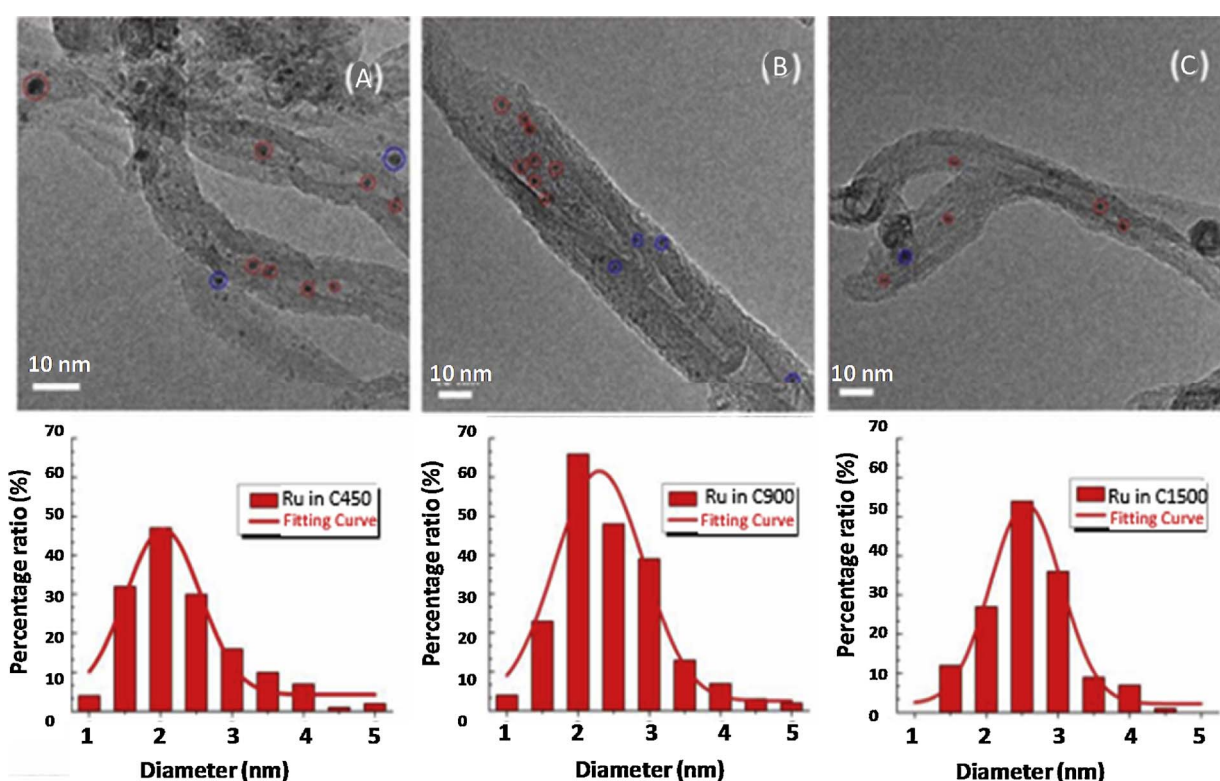


Fig. 6. TEM images and corresponding particle size distributions of catalysts consisting of 2 wt.% Ru supported on CNTs (A–C). They are shown for three different calcination temperatures, with Ru particles located inside the CNT indicated by red, and particles outside the CNT indicated by blue. (A) Calcination temperature of 450 °C (B) Calcination temperature of 900 °C (C) Calcination temperature of 1500 °C. (For interpretation of the references to colour in this figure legend, the reader is referred to the web version of this article.)

With permission to reprint from Ref [121], Copyright 2013, Royal Society of Chemistry.

precious metals, it is limited on N–H cleavage, while, for nonprecious metals, it is N_2 desorption. However, decomposition on metal amides is entirely different, which doesn't follow any of above mechanisms for metal catalysts. They mostly act as co-catalyst where either the amide first decomposes into metal, N_2 and H_2 and the metal reacts with ammonia to form metal amide again, thus continuing the cycle. In case of lithium amide, the process is a bit longer, as lithium amide forms lithium imide, which forms another complex, Li_4NH and then reacts with ammonia again to form Li_2NH . Due to the unique reaction mechanism, amide/imide catalysts seems more promising to enhance ammonia decomposition at relatively low temperature (< 450 °C). Instead, most of the studied metal catalysts achieve 100% conversion efficiency only when the temperature is above 600 °C.

3. Progress of ammonia decomposition catalysis

In addition to cost and scarcity, the preceding section indicated that by itself, a Ru catalyst does not offer acceptable low temperature activity for ammonia decomposition. The same is true of the other metallic and non-metallic catalysts considered in that section. Using the mechanistic understanding of ammonia decomposition on these catalysts, a number of studies have been undertaken seeking to develop better-performing catalysts. The various approaches that have been employed typically seek to alter the physical structure of the surface (e.g. expose crystal facets with greater catalytic activity), the electronic structure of the active site (e.g. reduce activation barriers) or both. These objectives have been approached by altering the support,

promotion or formulation of multi-component catalysts.

3.1. Ruthenium based catalyst

Recall, for example, that study of the ammonia decomposition reaction on different crystallographic surfaces of Ru showed that the activities over the Ru (0001) and (1110) crystal planes differ by an order of magnitude [33] and that DFT calculations suggest that B-5 sites are particularly active [77]. One means of altering the number of sites with one particular geometry is by varying the metal particle size, and several studies have taken this approach with Ru. Most often, studies of this type involve dispersing the active metal on some type of support. The support may simply stabilize the particles, but if the interactions are stronger, it may additionally alter the electronic structure of the supported metal. Ruthenium has been supported on a wide variety of supports including multi-walled carbon nanotubes (MWCNTs) [116], graphite [117], graphene nanocomposites [118], and several oxides [119].

When Ru is loaded onto CNTs, particles can be located on the external surface of the CNTs or on the internal surface. Surface functional groups on the CNTs strongly anchor metal particles, improving the metal dispersion of calcined catalysts [120]. Fig. 6, compare the particle size distributions when the annealing temperature is 450 °C (Fig. 6a), 900 °C (Fig. 6b), and 1500 °C (Fig. 6c). In those figures, Ru particles located inside the CNT are indicated by red and the particles outside CNT are indicated by blue [121]. As expected, the particle size distribution is observed to shift to larger particle diameters with increasing annealing temperature.

The optimum ruthenium particle size for the Ru/CNT catalysts remains debatable. There have been several studies on the effect of particle size on ammonia decomposition [122]. Some studies suggest that larger particles have a larger number of active sites, with an optimum size being between 3 and 7 nm. Also, it was found that a higher degree of support graphitization weakens the metal–carbon interaction, leading to larger particles, but showing better activity. However, a DFT study predicted an optimum Ru particle size of 2–3 nm for ammonia decomposition [123].

The particle size of Ru determines the concentration of B-5 type sites, and the 2–3 nm optimum corresponds to the maximum concentration of B-5 sites. The size of the Ru crystallites is also affected by the reduction temperature and the texture of the support being used. The metal dispersion can also be altered by using different supports such as graphene, carbon nanofibers (CNFs), nitrogen doped carbon etc. Graphene nanocomposite supports with Ru loadings of 18, 33 and 45 wt.% have been synthesized [118]. Even at a Ru loading of 50 wt.% the metal dispersion was uniform. This dispersion stabilization has been attributed to oxygen containing groups of the graphene nanocomposite that act as anchoring and nucleating sites for growth of Ru. The maximum metal loading that has been reported on CNT is 20 wt.%. Li et al. [118] attempted to use higher loadings on CNTs, but the Ru particles were found to form aggregates. Thus, because graphene has an edge over CNTs as a support, highly efficient dispersion of Ru even for metal loading of > 50 wt.% can be realized on graphene supports.

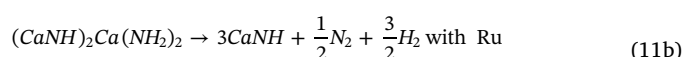
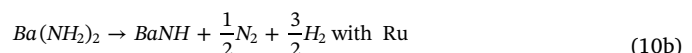
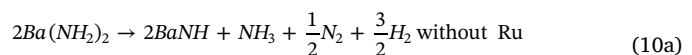
Another study showed that the particle size of Ru decreases with an increase in the pyridinic nitrogen content of the support. Pyridinic nitrogen is found at the edges of graphene sheets. The pyridinic nitrogen has an unbound electron, which anchors Ru³⁺ and prevents its agglomeration at higher metal loadings [35]. Recently, the catalytic performance of Ru dispersed on graphene has been investigated. Specifically, the conversion of ammonia on Ru/graphene nanocomposites was measured for different metal loadings. The conversion increases strongly with dispersion, but decreases with an increase in gas hour space velocity (GHSV) [118]. For example, at 450 °C, the conversion decreases from 91% to 62% when the GHSV is increased from 20,000 to 60,000 mL h⁻¹ g_{cat}⁻¹ while increasing the hydrogen production rate [118].

The preceding discussion indicates that the support may stabilize the metal particle size or morphology to maintain more active sites exposed. At the same time, the support is expected to affect the electronic structure of the supported metals. Another means of altering the electronic structure is by adding promoters. In 2004, Yin et al., for the first time, performed a detailed examination of the effects of various supports and promoters on Ru [36]. The conversion of Ru on CNT was better than that on oxide supports including MgO, Al₂O₃, and TiO₂. This study was followed by several others that examined modifications for increasing the conversion [34,36,55,56,66]. The approaches included using alkaline promoters, increasing the degree of support graphitization through thermal treatment, improving the metal dispersion on the support, optimizing the solvents used for catalyst synthesis by wet impregnation methods, and doping with nitrogen [37,41,43,55,117,124–126].

Noting that nitrogen desorption is the rate-limiting process over Ru because nitrogen is bound too strongly, effective promoters typically feature electron-donating groups. By donating electrons to the anti-bonding electronic states of the metal, the adsorbate–metal interaction (i.e. nitrogen–metal interaction) is weakened and nitrogen desorption becomes more facile. Therefore, basic promoters are favored over acidic promoters and electron withdrawing groups. Upon modification of Ru/CNT by doping alkali metal nitrates, the activities of the resulting promoted Ru catalysts are found to decrease in the order of K-Ru > Na-Ru > Li-Ru > Ce-Ru > Ba-Ru > La-Ru > Ca-Ru > Ru indicating that within the same group, the higher the electronegativity of the promoter, the lower the conversion of ammonia [116]. Since potassium doped Ru has the best performance, different precursors like KNO₃, KOH, K₂CO₃ were used to dope potassium onto Ru, and KOH was found to be the best precursor [116].

Cesium promoted Ru/MWCNT exhibited hydrogen production below 317 °C, which was a breakthrough for onsite hydrogen production from ammonia [127]. Two sets of catalysts were compared to study the effect of Ru and Cs loading. Cs acts as a strong electron donor on the surface of Ru and on the CNT support. This study confirmed that Cs/CNT does not act as a catalyst; Cs only enhances the activity of Ru/CNT. Upon increasing the Cs/Ru ratio, the decomposition rate initially increases and then decreases, showing a volcano type effect. The maximum in activity can be explained as a trade-off between site blockage by added Cs and promotion of the activity of the remaining unblocked sites. At low loading the promotional effect on unblocked sites predominates while at high loadings, the blocking effect prevails.

Recently, in 2016, the effects of several alkaline earth metal (IIA) amides Mg(NH₂)₂, Ca(NH₂)₂, and Ba(NH₂)₂ on the activity of Ru were investigated [128]. Although they are not very promising as promoters of Ru, the catalyst activities rank in the order of Ru–Ba(NH₂)₂ > Ru–Ca(NH₂)₂ > Ru–Mg(NH₂)₂. In addition, Ru–Ba(NH₂)₂ and Ru–Ca(NH₂)₂ catalysts have higher intrinsic activities (TOF) and lower apparent activation energies than those of Ru–Mg(NH₂)₂ and Ru/MgO catalysts, indicating that Ca(NH₂)₂ and Ba(NH₂)₂ may have promotional roles in facilitating ammonia decomposition when compared to Mg(NH₂)₂ and MgO [128]. Nonetheless, the conversion is not better than the Ru/MgO–CNT [34]. As indicated in Eqs. (10a), (10b), (11a), and (11b), the decomposition pathways of Ca(NH₂)₂ and Ba(NH₂)₂ are changed in the presence of Ru. Interestingly, lithium amide was not examined in that work.



3.2. Other metals

Because iron promoted with K_2O , CaO , SiO_2 and Al_2O_3 is active at temperatures above 400 °C for ammonia synthesis [46], it was initially considered as a potential catalyst for ammonia decomposition. Early studies on the use of iron for ammonia decomposition were focused on removing ammonia from hot flue gas during coal gasification and not on generating hydrogen. The high temperatures lead to iron sintering, but that can be prevented by using iron-based core-shell catalysts. The catalysis with iron is more complicated than with ruthenium because iron can form stable nitrides in presence of ammonia. Arabczak and Pelka [129] compared the activity of Fe and Fe_xN for ammonia decomposition and found that formation of surface nitrides reduces the ammonia decomposition rate. In addition, different phases of iron have shown different activity for ammonia decomposition [130].

It was found that the activity of iron is lower than that of ruthenium [125,130]. At low temperatures nitrogen desorption is rate limiting over iron catalysts, whereas at higher temperatures N–H cleavage limits the reaction rate [131,132]. The rate of decomposition of ammonia also depends on the partial pressure of ammonia and hydrogen, and is described by Temkin Pyzhev kinetics [133]. In a recent study conducted by Tuysuz et al. [134], catalysts were synthesized from iron phthalocyanine through a high temperature treatment. The activity was dependent on the size of the iron particle, which, in turn, was found to be a function of heating rate and temperature during catalyst synthesis. By using different gases like Ar and N_2 during pyrolysis, they found that heating under Ar gas at a high ramping rate would give rise to a high number of small sized and evenly distributed particles. This class of catalyst undergoes various phase transformations when exposed to ammonia, and the new crystalline phases that appear over time have activity comparable to ruthenium on carbon [134]. Following on this, subsequent studies added CNTs as a support for Fe and Co nanoparticles [135,136]. An ammonia conversion of 92% was achieved at 550 °C using Fe nanoparticles supported on carbon nanofiber, synthesized by CVD. Fig. 7(A) shows an HR-TEM of a single Fe nanoparticle supported on mica over a carbon nanofiber that was synthesized using a wet impregnation method. Its EDS is shown in Fig. 7(B). Fig. 7(C) shows the HRTEM of an Fe nanoparticle cluster on carbon nanofiber with the particle size distribution shown in Fig. 7(D) [62].

Duan et al. [62] tried to control catalytic properties by tuning the Fe nanoparticle size. The particle size distribution was found to be uniform with the use of mica as the support. The ammonia conversion is compared at different temperatures for 3.5 wt.% Fe–CNFs/mica, 3.5 wt.% CNFs, neat mica, and 3.5 wt% Fe/mica in Fig. 8(A) [62]. The best conversion is observed for 3.5 wt.% Fe–CNFs/mica followed by 3.5 wt.% Fe/CNFs and 3.5 wt.% Fe/mica. Pure mica performs poorly, indicating its role as support/promoter is much more prominent than its role as a catalyst. The conversion over the Fe-CNF/mica catalyst increased for the first 220 min at 550 °C and then became stable as shown in Fig. 8(B) [62]. Thus, for iron-based catalysts, controlling the particle size and using supports like carbon nanofiber can improve catalytic efficiency. However, iron-based catalysts have not shown significant activity for ammonia decomposition at lower temperatures (< 450 °C).

Ganley et al. [52] used DFT to predict the activity of several metals. On the basis of turnover frequency, Ni has better activity than Pd and Pt, but it is considerably less active than Ru and Rh. When supported on CNTs, Ni shows relatively poor performance upon comparison to Fe/CNT and Ru/CNT. In a kinetics study of ammonia decomposition by Ni nanoparticles, Zhang et al. [137], observed a strong correlation between the particle size of nickel and its activity for ammonia decomposition. Later, it was found that decreasing the size of nickel particles supported on alumina leads to an increase in TOF. Studies of the dissociation activity of ammonia on different crystallographic faces of Ni, e.g. (110) and (111), are consistent with the findings of Zhang et al. and others [138,139]. Okura et al. [59] studied the dispersion of Ni on supports like Al_2O_3 , CeO_2 , Y_2O_3 , and other rare earth oxides. Ni on

Y_2O_3 exhibited the best conversion among all other rare earth oxide-supported Ni catalysts, though alumina has higher surface area. A conversion of 87% at 550 °C was obtained for Ni/ Y_2O_3 [59], and it was found to be very stable for 50 h. The rate of ammonia decomposition on Ni supported on rare earth oxides was found to decrease with increasing partial pressure of hydrogen. The magnitude of the inhibition was in the order of Ni/Al_2O_3 (0.88) > Ni/CeO_2 (0.86) > Ni/Sm_2O_3 (0.66) > Ni/Y_2O_3 (0.48) > Ni/Gd_2O_3 (0.46). Thus, although Al_2O_3 has a larger surface area than Y_2O_3 , the conversion of ammonia on alumina-supported Ni is smaller due to the strong inhibitive effect of hydrogen.

Liu et al. [140], chemically modified nickel with alumina and ceria. A mixture with an Al^{3+}/Ce^{3+} ratio of 9 was optimum, resulting in a 10-fold increase in the surface nickel atoms per gram of catalyst compared to the neat micro-fibrous nickel substrate. A 0.9 mL bed of the modified catalyst was capable of an ammonia conversion efficiency greater than 99% at 650 °C throughout 100 h of continuous testing [140]. Ni wires (210 kJ/mol) had the largest activation energy, followed by Ni films (180 kJ/mole) and Al/Ce modified micro-fibrous nickel (103–105 kJ/mole). However, the lowest activation energy is for nickel supported on silica and HY zeolite (80–90 kJ/mole), indicating that these supports actually enhance the activity of the nickel catalyst for ammonia decomposition. When carbon supports were used for Ni, better activity was observed on MWCNTs than on activated carbon (AC). This might be due to the uniform distribution of Ni nanoparticles on MWCNTs (Fig. 9A) [141] compared to AC (Fig. 9B). At 500 °C and a GHSV of 6000 h^{-1} , NH_3 conversion on Ni/MWCNT has been reported to be 57.64% compared to 24.83% conversion of NH_3 over Ni/AC [141].

Investigation of cobalt as a monometallic catalyst for decomposition of ammonia paralleled that of iron [135] and nickel. The roles of supports like MWCNT and various promoters were investigated on cobalt as well. At 500 °C, the conversion on Co/MWCNT was 60.0% compared to 14.8% for iron and 25.4% for nickel [142]. The effect of thermal control has been investigated [143], and it has been observed that even choice of cobalt salt and calcination condition affect the properties of the synthesized catalysts [142]. The best activity reported for a cobalt catalyst at low temperature was obtained using a triply promoted cobalt oxide catalyst. Specifically, the cobalt oxide catalyst (II and III), promoted with calcium oxide, potassium oxide, and aluminium oxide, showed a stable conversion of 100% at 525 °C [144]. In order to attain complete conversion of ammonia, the precipitation temperature and the quantities of the promoters had to be optimized. The addition of alumina enhanced decomposition at lower temperature. Table 2 shows the proportion of the oxides and how they were varied during synthesis of each catalyst in order to determine their individual roles [144]. The activity strongly depends on the crystallite size in addition to the nature of support and promoters. Fig. 10(A) shows the degree of ammonia conversion for the three catalysts in Table 2. SEM images of the ZBPA1-C catalyst are shown in Fig. 10(B) [144]. Another study revealed that the triply promoted catalyst forms a typical 3D bridge structure that might be responsible for the enhanced activity [63].

Thus, among Fe, Co, and Ni, the use of CNT or CNF as support and alkali promoters results in significant activity improvement at temperatures greater than 600 °C, but the conversion around the target temperature of 450 °C still lags that of Ru. Nanoparticles of Fe, Ni, and Co dispersed on an alumina matrix prepared by coprecipitation were studied at a 90% loading. Though there is considerable conversion at 500 °C, 99% conversion is achieved only at 600 °C [145]. The increase in conversion with increase in metal loading for Fe and Co is shown in Fig. 11(A) and (B) respectively [145].

3.3. Multi-component and composite catalysts

It has already been noted that for ammonia synthesis, catalytic activity is a function of nitrogen binding energy [146]. For ammonia synthesis, Jacobsen et al. identified the optimal catalyst at different

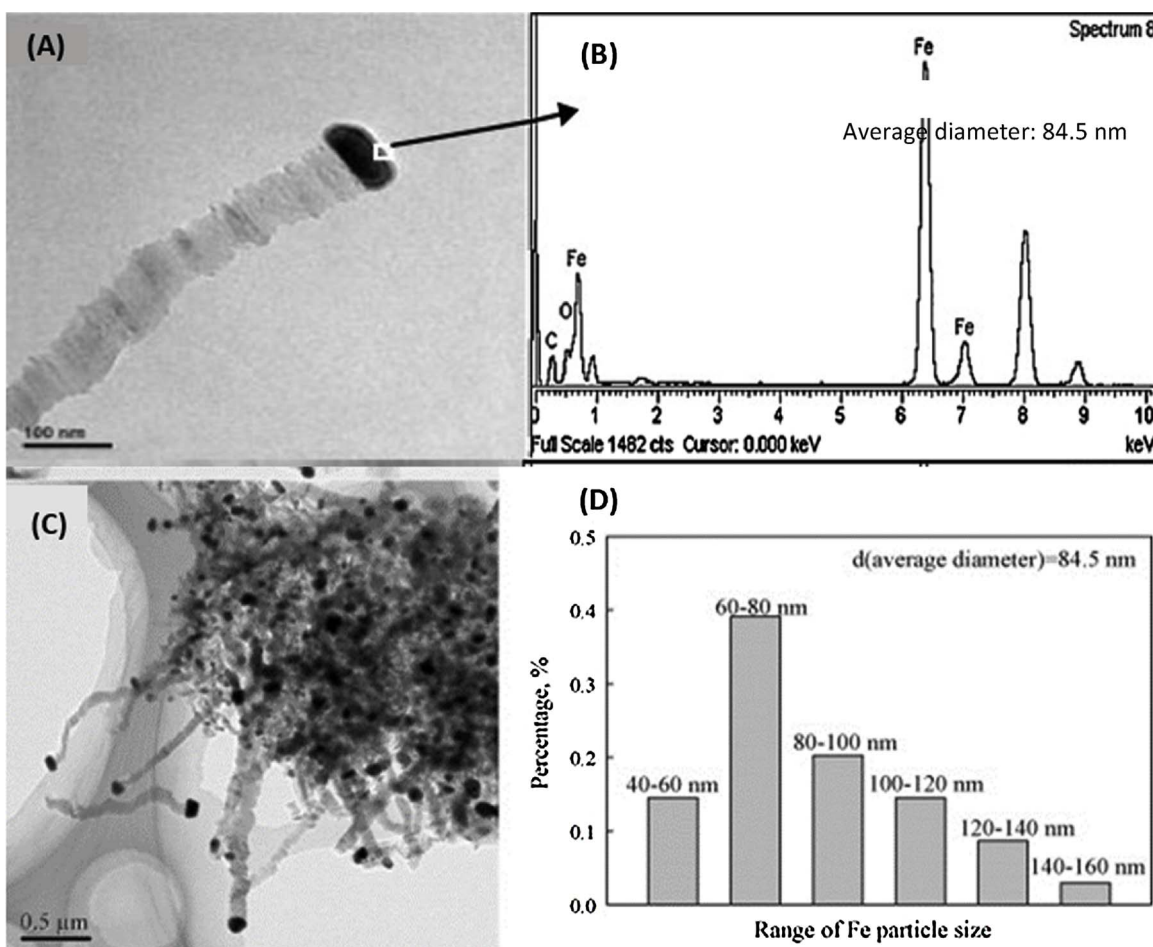


Fig. 7. (A) HR-TEM of an Fe nanoparticle on mica/carbon nanofiber, (B) EDS of the Fe nanoparticle on mica/carbon nanofiber, (C) HR-TEM of a cluster of Fe on CNF, and (D) Particle size distribution of cluster of Fe on CNF.
With permission to reprint from Ref [62], Copyright 2011, Elsevier.

temperatures, pressure, and gas composition. Similarly, for ammonia decomposition Ru has the optimal heat of chemisorption among single metals [147]. To obtain a lower activation energy than Ru, an optimized combination of nonprecious metals with different nitrogen binding energies was required.

3.3.1. Bimetallic catalysts

It has been demonstrated that molybdenum, a metal with high

nitrogen binding energy combined with cobalt, a metal with a low binding energy by Duan et al. [64] and traces of Co added to Fe by Zhang et al. [135] resulted in improved activity for ammonia decomposition. Table 3 illustrates how the activation energy for the single-component catalysts can differ from that of their composites. Pure Fe metal has a very high activation energy, which decreases upon combination with Co. It also decreases when Fe is synthesized on an electron donating support like CNT/CNF. Similarly, the activation energy of

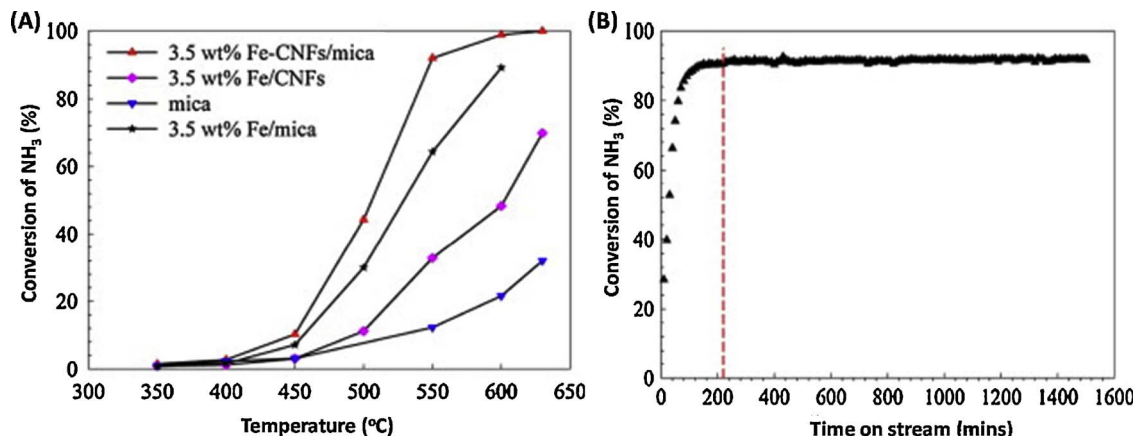


Fig. 8. (A) Comparison of conversion of ammonia with temperature for Fe with mica supported on CNF, Fe without the mica support and without the CNF support to understand the importance of mica and CNF. (B) Conversion as a function of time for Fe supported on mica/CNF.
With permission to reprint from Ref [62], Copyright 2011, Elsevier.

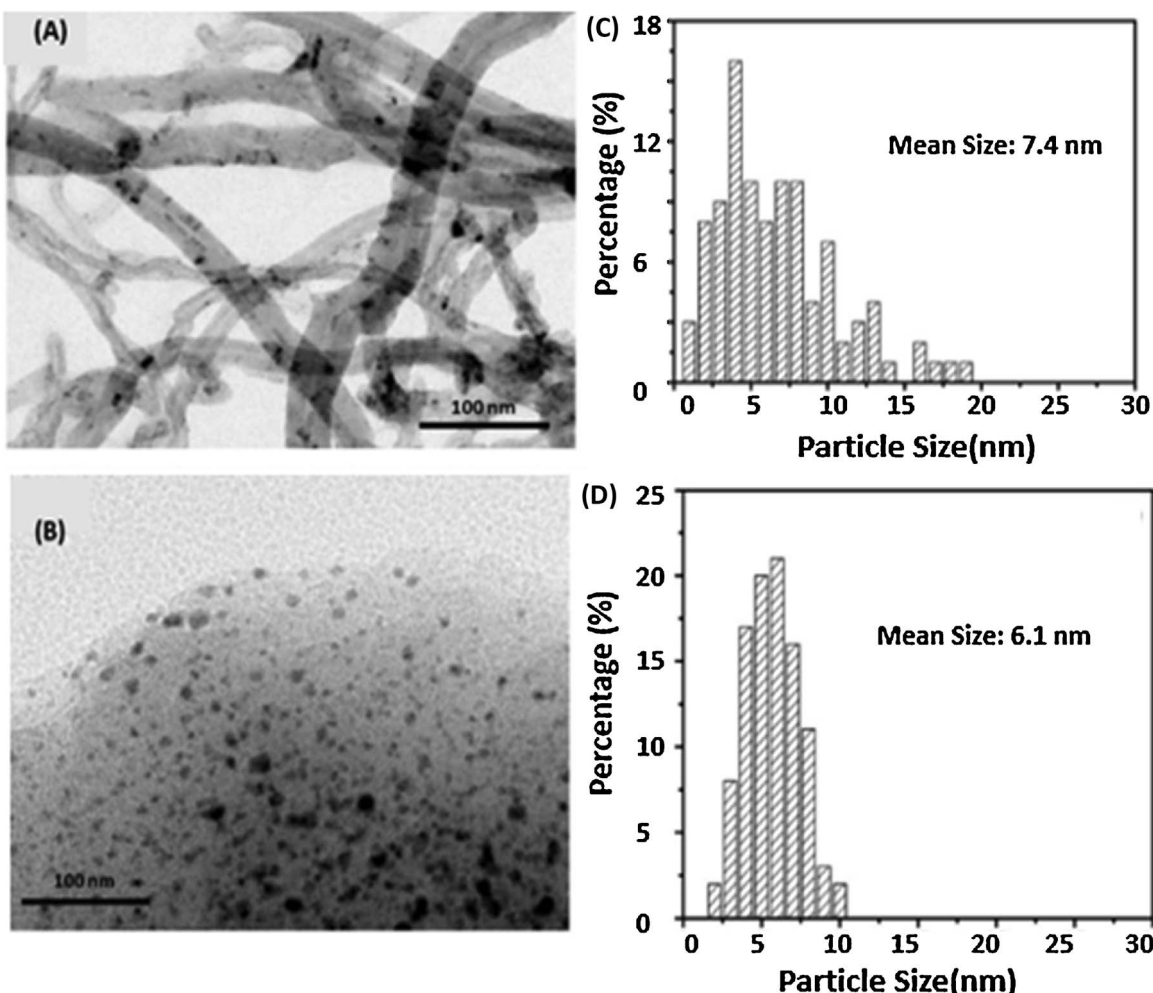


Fig. 9. TEM images of (A) Ni particles on MWCNTS and their particle size distribution in (C) (B) Ni particles on AC and their particle size distribution in (D). With permission to reprint from Ref [141], Copyright 2014, Elsevier.

Table 2
Variation of Promoters (Triple Oxides) of each catalyst.
With permission to reprint from Ref [144], Copyright 2016, Elsevier.

Sample ID	Promoters used	Oxide Content [% mass]		
		K ₂ O	Al ₂ O ₃	CaO
ZBPA1-A	K ₂ O, Al ₂ O ₃	0.42	2.8	
ZBPA1-B	K ₂ O, CaO	0.56		2.58
ZBPA1-C	K ₂ O, Al ₂ O ₃ , CaO	0.55	2.8/4.1	2.4

nitride imide composite is lower than that of nitrides alone. Similarly, Fe-Co/CNT [136], Fe-Ni/Al₂O₃, and Ni-Fe [42] alloys were found to show better activity than the single metals as shown in Fig. 12(A) and (B), where the productivity/activation energies and relative activities are compared for various bimetallic catalysts [135].

Decomposition on a bimetallic Pd-Cu(111) surface was also studied theoretically using DFT [152]. The adsorption energy calculations on the bimetallic surface indicated that doping the metal surface with another metal led to an energy reduction. Adsorption is favored on different sites based on the nature of the metal. This is seen in a theoretical study by Jiang et al. [152] where different sites for NH₂ attachment were observed for the surface of a bimetallic alloy (Pd-Cu) depending on the face exposed to the adsorbate. When Pd forms the top surface layer, the NH₂ attachment occurs at the fcc site (Fig. 13A), while the adsorption occurs at a bridge site when Cu forms the top surface layer (Fig. 13B) [152]. Through their calculations they also

determined that the energy barrier for NH dehydrogenation is much higher than that for NH₃ and NH₂ [152], indicating dissociation of NH as the rate determining step.

Besides Fe-Co, Pd-Cu, Fe-Mo bimetallic catalysts supported on commercial zirconia and alumina showed significant improvement compared to single metal [153]. However, such synergistic effects is obvious at high temperature, their conversion at low temperature (< 550 °C) is less than 20% even when supported with zirconia and alumina. Thus, the bimetallic catalyst discussed so far are not suitable for onsite H₂ generation even though they have been structurally modified with different supports. However, their performance is better than their monometallic counterpart.

3.3.2. Bimetallic nitrides

Though bimetallic alloys are better than monometallic catalysts, the improvement it is not sufficient to facilitate ammonia decomposition at temperatures lower than 450 °C. Bimetallic nitrides have also been examined. Conversion of ammonia on MoN was 99% at 600 °C. When Co metal was infused into MoN, the conversion at lower temperatures increased, but the temperature for complete 100% conversion remained the same (Fig. 14A). It has been reported that increasing the loading of Co from 1 to 3 wt.% increases the conversion at temperatures of 450–550 °C. This is due to the formation of Co₃Mo₃N in the cobalt containing samples [154]. Fig. 14(B) compares the activity of oxide and nitride catalysts [154], showing similar activity (close to 100%) after initial activation at a relatively high temperature (650 °C). Because oxides would be eventually converted to nitrides under NH₃

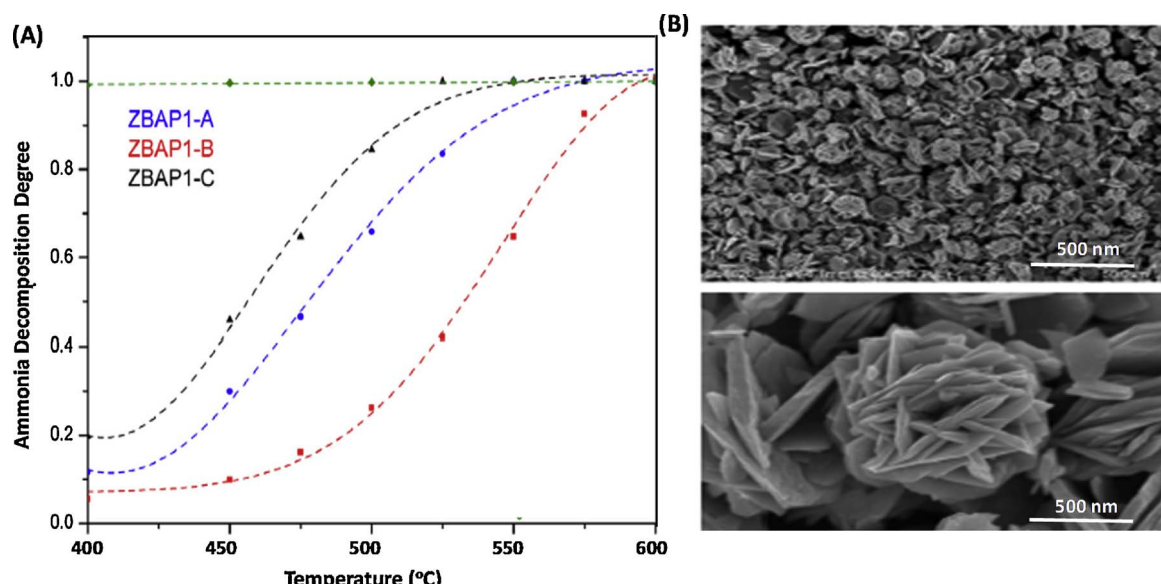


Fig. 10. (A) Variation of degree of decomposition of ammonia for three different catalysts with different loading of triply promoted catalyst and (B) SEM images of the Co/MWCNT catalyst promoted with triple oxides as shown in Table 2.

With permission to reprint from Ref [144], Copyright 2016, Elsevier.

atmosphere at high temperatures.

Leybo et al. studied the decomposition reaction over nickel molybdenum nitride (NiMoN) and suggested that increasing the nitride phase content by 37 wt.% doubles the ammonia conversion at 550 °C [155]. This study focused on finding the effect of different preparation techniques and the role of precursors in the activity of the resulting nitrides. The onset of ammonia conversion was 400 °C, but again complete conversion was only achieved at 650 °C. Nonetheless, this study was successful in elucidating the dependence of morphology, specific surface area, and average particle size on the production methods and the initial precursor compositions. The present trend is to use the synergy between different nitrides and imides in composite catalysts for low temperature conversion, *vide infra*.

3.3.3. Mixed imide and nitride-imide catalysts

Recall from Fig. 5 that the mixed amides, $\text{Li}_2\text{Ca}(\text{NH})_2$ and $\text{Li}_2\text{Mg}(\text{NH})_2$, were more active at low temperature than the single component, non-stoichiometric Li_2NH . Decomposition of lithium imide was studied by Zhang et al. [113] using temperature program desorption, and the

Table 3

Comparison of catalytic activation energies for low temperature decomposition of ammonia.

Catalyst	Activation Energy (kJ/mole)	Reference
Fe	147	[44,136,148]
CoFe_5/CNT	105–107	[136]
Fe-CNF/mica	93.5	[62]
Ru	89.4	[149]
Ru/CNT	72.2	[150]
Li_2NH	150.9	[149]
$\text{Ru-Li}_2\text{NH}$	53.2	[149]
MnN	138.6	[150]
$\text{MnN-2Li}_2\text{NH}$	76	[150]
Mn_6N_5	138	[151]
$\text{Mn}_6\text{N}_5\text{-xCaNH}$	85	[151]

kinetic analysis showed that the activation energies are very high: 754.2 kJ/mole for the first step and 754.2 kJ/mole for the second step. It decomposes at temperatures between 550 and 800 °C, which is above the range of our interest for ammonia decomposition catalysts

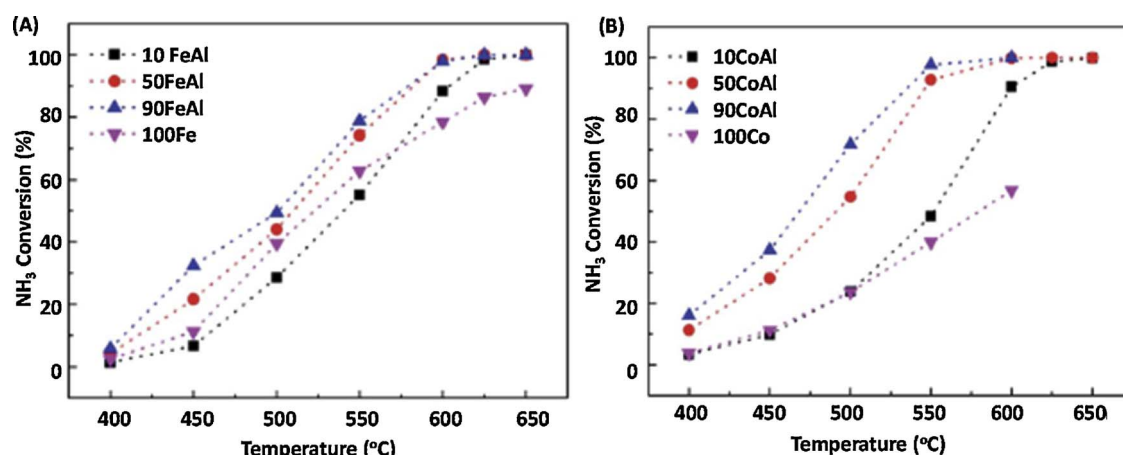


Fig. 11. (A) Comparison of ammonia conversion with temperature for different loadings of Fe nanoparticles on an alumina matrix. As the metal loading increases, the conversion increases at a particular temperature. (B) Dependence of ammonia conversion upon temperature for Co nanoparticles loaded on an alumina matrix. As the metal loading increases, the conversion again increases at a particular temperature. The conversion over CoAl is much better than over FeAl at lower temperatures.

With permission to reprint from Ref [145], Copyright 2015, Royal Society of Chemistry.

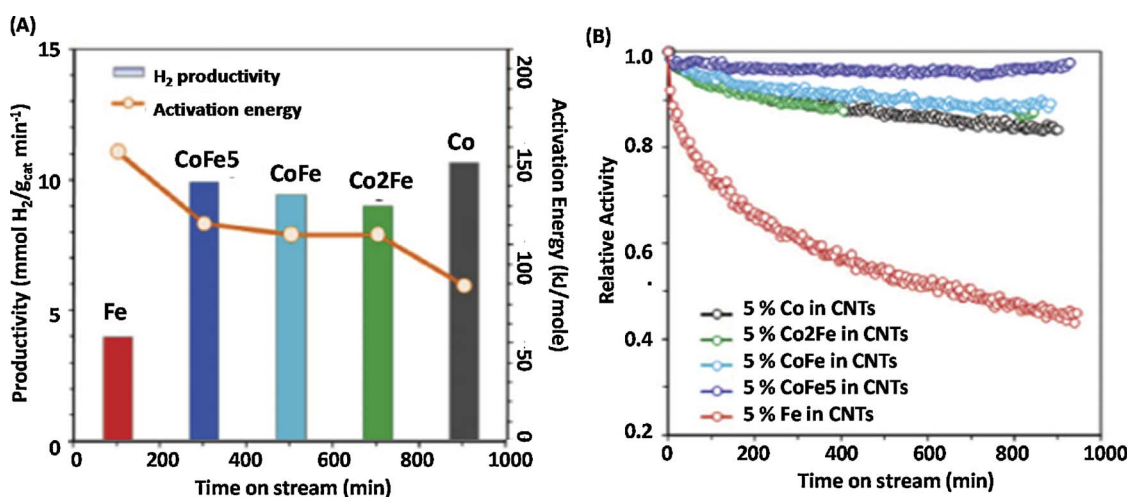


Fig. 12. (A) Comparison of hydrogen productivity of bimetallic FeCo catalysts with different loadings of Co. Fe has a very low activity for ammonia decomposition, but FeCo alloys have better activity. (B) Relative activity variation of different FeCo catalysts with time. With permission to reprint from Ref [136], Copyright 2008, American Chemical Society.

(< 450 °C). Hence, unlike sodium amide, its stability would not be a concern. Since it does not decompose, the nitrogen and hydrogen evolution is from decomposition of ammonia. However, with higher concentrations of NH₃, the reverse reaction is favored, in which lithium imide reacts with ammonia to form lithium amide and the lithium amide will generate ammonia again [150].

The limitation of most light metal amides is the difficulty of containing them within the reactor due to their low melting point. Sometimes U-shaped reactors or stainless steel tank reactors are preferred for carrying out these reactions because in a U tube reactor or tank the catalyst will be contained even if it melts. Alternatively, Makepeace et al. [115] reported that lithium calcium imide (see Fig. 5) remains solid when heated under argon to the temperature where ammonia conversion is observed. When heated under argon, lithium imide cannot convert back to lithium amide. This helps to contain the catalyst within the reactor. Similarly, in their studies on lithium calcium imide, when argon was used, the recovery of lithium calcium imide after reaction was 95%. In their study of lithium magnesium imide, argon was not used and the mass recovered after reaction was less than 5%. Lithium calcium imide exhibits the best reported conversion among the amide-imide catalysts that have been examined so far [115].

Recently, Ni-doped LiNH₂/C was found to be active at 400 °C showing 53% conversion at that low temperature [156]. They attempted to confine LiNH₂ in nanoporous carbon to form a nanocomposite with applications for hydrogen storage as well as for

catalytic decomposition of ammonia. The degree of ammonia conversion was determined by monitoring the reduction in the intensity of the ammonia signal and the increase in the signals for hydrogen and nitrogen in a TPD-MS instrument. The inlet gas flow was 10% NH₃ in He. They used two supports for their nanocomposite catalyst, one of which was nanoporous graphite (npg) and the other was carbon xerogel, which they termed as CX. The performance of 5 wt.% of Ni on CX nanocomposite was found performing better than LiNH₂/CX nanocomposite. Due to the possible reactions between lithium amide and the carbon at high temperature, using carbon support might not be suitable to enhance stability of amide catalyst. However, it would require more experiments to confirm this.

A more recent development is the use of composites of lithium amide-imide with transition metal nitrides. Composites consisting of transition metal nitrides and 1A group amides/imides have shown much higher catalytic activity when compared to metal nitrides alone [157]. Guo et al. [57] made an interesting observation after intentionally impregnating Fe on LiNH₂. They found the catalytic activity is much enhanced relative to Fe/CNTs or Fe or Li₂NH individually. They observed the composite to be active at 350 °C, ca. 100 °C lower than Fe₂N and Li₂NH. It was proposed that Fe₂N reacts with Li₂NH at temperatures below 227 °C, giving rise to H₂ and Li₃FeN₂. It was further proposed that at temperatures above 227 °C, Li₃FeN₂ decomposes back to lithium imide, nitrogen and iron nitride. This observation became a driving force behind investigation of the synergy between nitrides and imides as new class catalysts for ammonia decomposition.

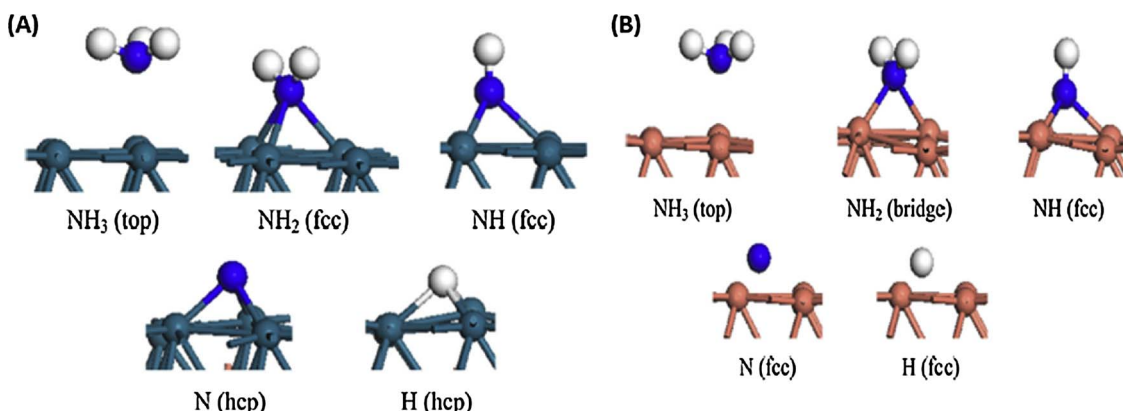


Fig. 13. (A) Decomposition mechanism on Pd-Cu (111) facet, and (B) Decomposition on Cu-Pd (111). They differ in the site of adsorption and in the site for dehydrogenation. With permission to reprint from Ref [152], Copyright 2016, Elsevier.

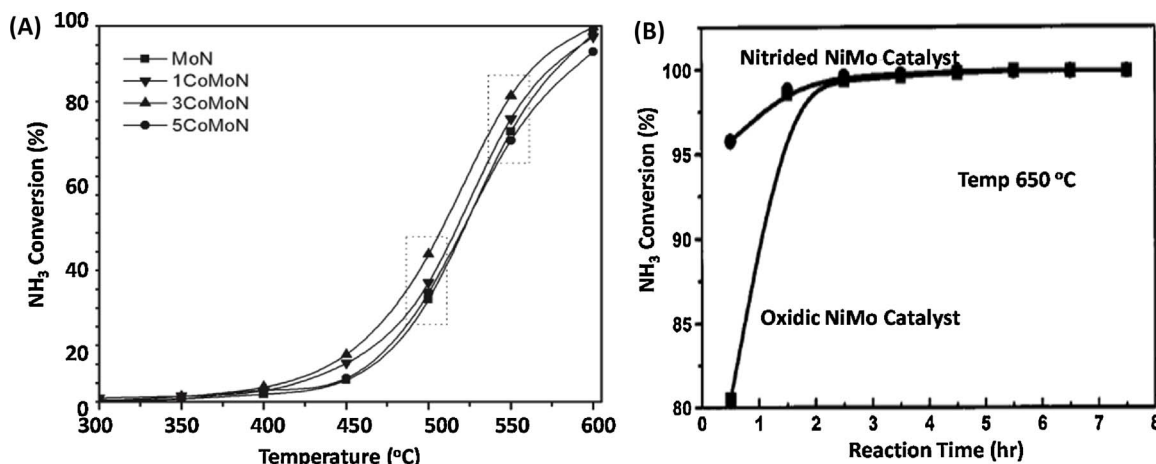
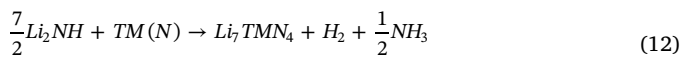


Fig. 14. (A). Variation in conversion of ammonia with temperature for different CoMoN catalysts. With permission to reprint from Ref [154], Copyright Royal Society of Chemistry. (B). At a GHSV of 1800 hr⁻¹ a nitrided NiMo catalyst has almost complete conversion at 650 °C compared to oxidic catalyst. With permission to reprint from Ref [54], Copyright 2000, American Chemical Society.

While a synergistic effect between alkali metal imides and transition metal nitrides has been observed, the catalytic mechanism appears to be quite different from the mechanism over the individual components. The imides and nitride composite first forms a complex evolving hydrogen in the process. The complex further reacts with ammonia to give back the nitride, imide and nitrogen. Guo et al. in 2015 reported such mechanism of ammonia decomposition on MnN-Li₂NH [158]. They used a quartz tube fixed bed reactor at ambient pressure. In their reactor, below 477 °C, neither MnN nor Li₂NH had considerable activity. However, for a composite catalyst consisting of a MnCl₂ to LiNH₂ ratio of 1:23, decomposition activity was observed at 350 °C. XRD characterization of the used catalyst indicated the formation of Li₇MnN₄. It is suggested that lithium amide and metal nitrides form ternary metal amides Li₇MN₄, (Eq. (12)). Then it is decomposed in a cyclic process as shown in Eq. (13). Thus, the net result is the decomposition of ammonia into nitrogen and hydrogen as in Eq. (14) [150].



The apparent activation energy over MnN-Li₂NH is similar to that for Ru/CNTs. At a ratio of 1:2 for MnN to Li₂NH, the hydrogen production rate is 37.5 mmol_{H2} g_{cat}⁻¹ min⁻¹ at 500 °C. This is ~40 times higher than MnN alone, and even superior to the highly active Ru-based catalysts under the same conditions. A comparison of the rate of ammonia decomposition for different ratios of MnN-Li₂NH is shown in Fig. 15(a) [150]. There is not much difference in the rate when the ratio of MnN to Li₂NH is varied from 1:0.2 to 1:23. Fig. 15(b) further compares the stability of three MnN-Li₂NH catalysts for 8 h. However, the stability of the composite MnN:Li₂NH (1:23) is not reported. This is perhaps due to the fact that higher lithium imide content would increase the formation of lithium amide as shown in Eq. (15), leading to a stability concern. This is another reason why MnN-0.2Li₂NH is more stable than MnN-2Li₂NH as shown in Fig. 15(b). Formation of lithium amide can be prevented by either increasing the temperature of reaction or by reducing the pressure of ammonia.



Guo et al. further compared the degree of conversion of ammonia using different weight hourly space velocity (WHSV), which is the weight of feed flowing per weight of catalyst per hour. Typically, they

used catalytic loading of 0.5 g. At a WHSV of ammonia of 20,000 mLg_{cat}⁻¹ h⁻¹, the composite MnN-Li₂NH catalyst with a ratio of 1:2 was found to have much lower stability than at 8500 mLg_{cat}⁻¹ h⁻¹. Higher the WHSV, higher is the partial pressure of ammonia. This leads to the formation of LiNH₂. As LiNH₂ decomposes around 360 °C, it affects the stability of the composite catalysts. Therefore, to achieve high conversion at low temperature using nitride imide composite, the partial pressure of ammonia used is as critical as the reactor design. However, if the composite is optimized and the degree of conversion is very high initially, it prevents formation of lithium amide, as shown in Fig. 15(b). For MnN-0.2Li₂NH, even at 20,000 mLg_{cat}⁻¹ h⁻¹, the catalyst is stable for 8 h.

Similarly, Yu et al. reported that Mn₆N₅ and CaNH individually exhibit poor activity for ammonia decomposition, but they show a synergistic effect together which reduced the overall activation energy by 40% for ammonia decomposition. They also reported their study using pure ammonia and a flow rate of 30 mL min⁻¹ for a catalytic loading of 50 mg [151]. Fig. 15(c) shows the degree of conversion of different composites of CaNH and Mn₆N₅. Though they attain complete conversion at higher temperature, the synergy between CaNH and Mn₆N₅ cannot be ignored. Like Guo et al., they also related the role of formation of complex to the increase in activity. They mentioned that the formation of an intermediate like Ca₆MnN₅ significantly decreases the activation energy for ammonia decomposition. Mn₆N₅ and CaNH have also been tested for ammonia decomposition activity but their activity below 500 °C is insignificant. To investigate the role of Ca as an alkaline promoter, they also used CaO as a support on Mn₆N₅. On using CaO as a support, though the degree of conversion improved, the performance of Mn₆N₅-CaNH composite was still the best. However, compared to the performance of MnN-Li₂NH, the conversion was lower using CaNH.

Compared to other alkali and alkaline earth metal imides that have been studied, lithium has the highest synergistic effect with MnN, with activities decreasing in the order Li > Ca > K > Na (Fig. 15d). A primary goal of researchers currently working in this area is to bring down the temperature for decomposition of ammonia further while achieving a conversion close to 100%. Guo et al. [57] studied various transition metal nitrides and their composite with the highly synergistic lithium imide. They measured the conversion in ammonia decomposition experimentally and calculated the corresponding Gibbs free energy theoretically. The data for various transition metals are presented in Fig. 16 [57], highlighting their activity for ammonia decomposition as well as providing insight into the variation of the Gibbs free energy change for the two important steps of generating H₂ and N₂, respectively.

The performance of Li₂NH-TM(N) composites with transition metals

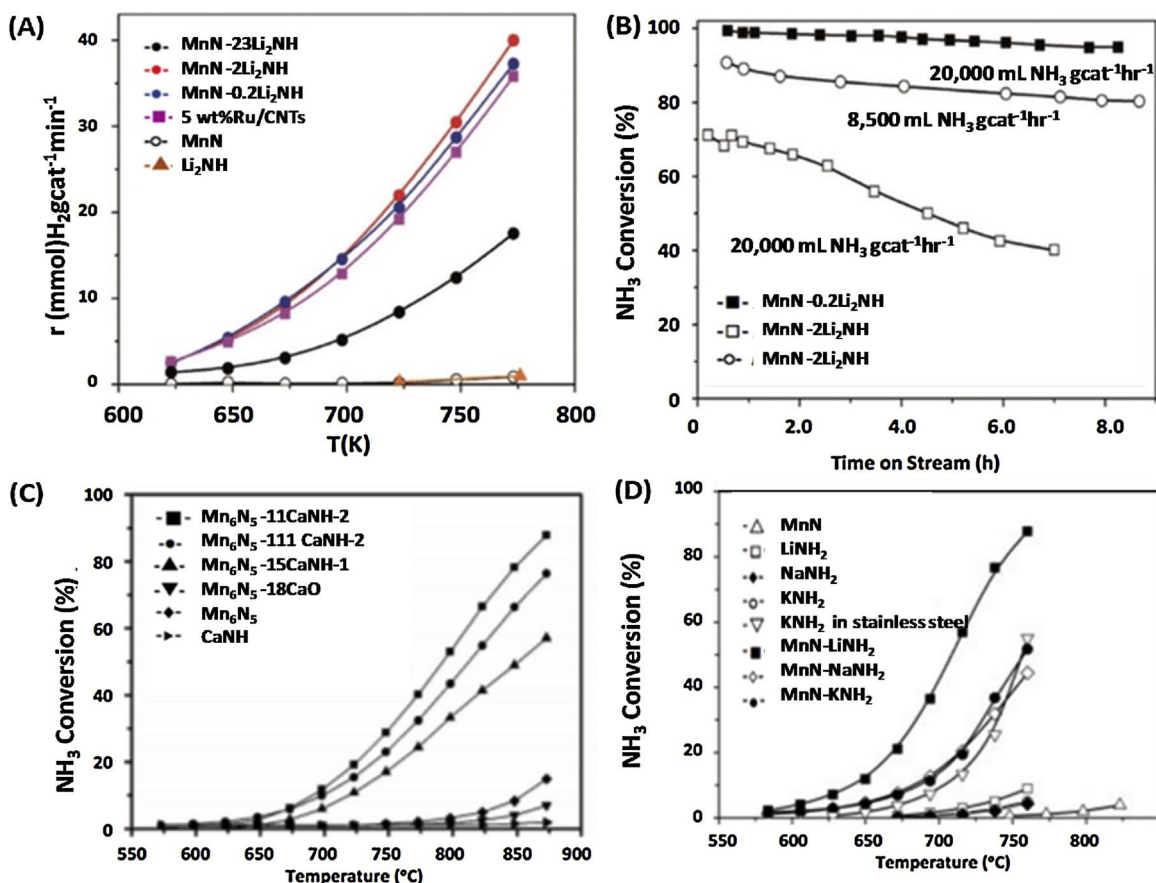


Fig. 15. (A) Comparison of the rate of decomposition of ammonia as a function of temperature for different molar ratios of composite of MnN-Li₂NH to those of MnN and Li₂NH alone. Reaction conditions: catalyst precursor loading, 30 mg; NH₃ flow rate, 30 mLmin⁻¹. (B) Stability of different ratios of MnN-Li₂NH composite catalysts under different WHSVs. With permission to reprint from Ref [150], Copyright 2015, American Chemical Society. (C) Variation of conversions of NH₃ over composite MnN-CaNH catalysts. Reaction conditions: sample loading 50 mg, flow rate of pure NH₃ 30 mLmin⁻¹. (D) Comparison of conversion of ammonia as a function of temperature for alkali metal amides like NaNH₂, KNH₂, LiNH₂, to nitride-imide composite catalysts and MnN alone. Reaction conditions: catalyst precursor loading, 30 mg; NH₃ flow rate: 30 mL min⁻¹. With permission to reprint from Ref [151], Copyright 2016, Royal Society of Chemistry.

from Ti to Cu is shown in Fig. 16a [57]. The general activity follows the trend: Mn > Co = Fe > Cr > Ni > V > Cu > Ti. All of the Li₂NH-TM(N) catalysts that were studied exhibited catalytic activity for NH₃ decomposition at temperatures above 350 °C. In Fig. 16b, hourly rates of NH₃ conversion at 500 °C for the Li₂NH-TM(N) are compared with those of the early 3d TMN, CNT-supported Co, Ni, Cu and Ru and 5 wt. % Ru/Al₂O₃. CrN-Li₂NH, Fe₂N-Li₂NH, MnN-Li₂NH, and Co-Li₂NH have activities significantly higher than that of 5 wt.% Ru/Al₂O₃ [36]. The ratio of TMN:Li₂NH ratio was kept at 0.9 to allow the formation of LiTMN. According to the Gibbs free energy changes shown in Fig. 16c, MnN is the most promising catalyst for the concurrent occurrence of the cyclic reactions that produce and consume the ternary nitride. It is followed by Cr, Cu, Co and Ni, while V has exceptionally good capability to generate H₂ (Fig. 16d). The use of electron conductive supports may help vanadium nitrides overcome the positive energy barrier for the nitrogen-producing reaction. Kinetic studies of ammonia decomposition on vanadium nitride have been reported [159], but its synergy with amide or amide is yet to be reported. Fig. 16b shows a volcano plot with Mn at the peak. MnN-Li₂NH has already shown a higher activity than 5% Ru/CNTs, and this can be a major factor motivating additional theoretical and experimental studies to understand the reason for the maximum shifting from Ni (for the CNT-supported, single component catalysts) to Mn (for the composite catalysts). Nonetheless, the onset temperature for ammonia decomposition is as low as 350 °C, which is very promising for onsite fueling station applications provided the stability and activity of the catalysts are optimized.

4. Development of reactor technology for ammonia decomposition

There are extensive reviews based on the state of the art reactor technology for ammonia decomposition to generate hydrogen for PEM fuel cells [160]. Rather than providing a chronological order of the development of reactors for ammonia decomposition, we gave brief highlights of importance and challenges of reactors designed for achieving 100% conversion efficiency under economic conditions. Although catalysts can improve reaction kinetics, heat and mass transfer limitations can be overcome by optimizing the reactor and relevant conditions. U. S. DOE didn't use ammonia for onboard hydrogen storage based on the inability of existing fixed bed reactors, which failed to satisfy the specified technical targets such as weight, volume, start-up time, etc [161]. Size and weight limits application for portable fuel cell devices. Table 4 highlights the broad class of reactors used for ammonia decomposition.

The catalytic membrane reactors have been tested with Ru and Ni catalysts supported on alumina. However, they have not been tested with any nitrides, amide/imide or nitride imide composite catalysts yet. In general, beside the reactor type, the flow rate of ammonia, partial pressure, dimensions of the reactor, pressure drop, temperature gradient, sweep gas, etc play important roles in governing overall catalyst performance. Though some catalytic membrane reactors have demonstrated significant performance at 450 °C, they have not been optimized with the best catalyst yet. For other microreactors, it was reported that conversion up to 99% was achieved at temperature around 600 °C.

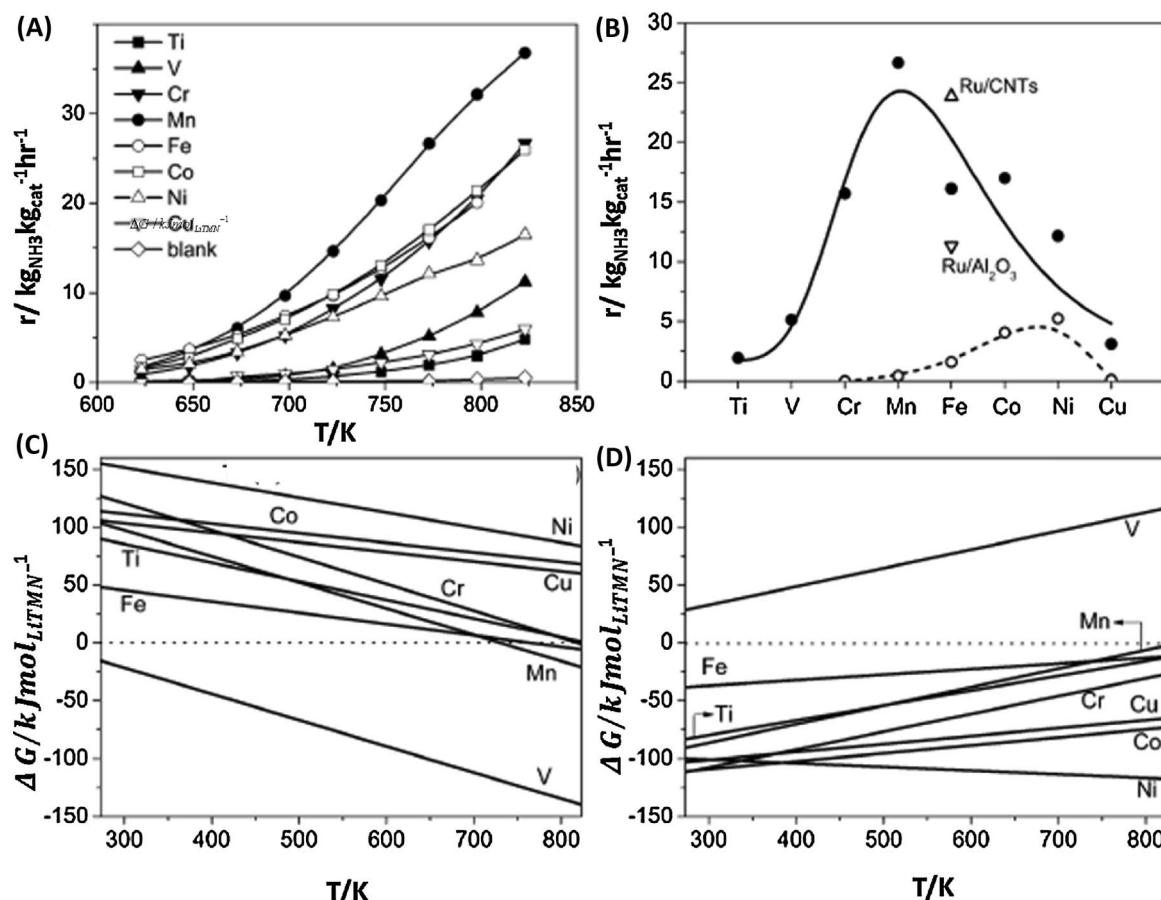


Fig. 16. Catalytic activities and thermodynamic analyses of $\text{Li}_2\text{NH-TM(N)}$ composite catalysts. (a) Variation of the rate of decomposition of ammonia with temperature for composites with transition metals from Ti to Cu. Reaction conditions: 30 mg catalyst, NH_3 flow rate 30 mL min^{-1} . (b) NH_3 conversion rates at 773 K for $\text{Li}_2\text{NH-TM(N)}$ composite catalysts (•) vs. rates over early 3d TMN and CNT-supported Co, Ni, Cu (○) and Ru (Δ). The activity of 5.0 wt.% Ru/ Al_2O_3 (▽) is also shown. Temperature dependence of the Gibbs free energy changes for the reactions (c) $\text{TM(N)} + \text{Li}_2\text{NH} \rightarrow \text{LiTMN} + \text{H}_2 + (\text{NH}_3)$ and (d) $\text{LiTMN} + \text{NH}_3 \rightarrow \text{Li}_2\text{NH} + \text{TM(N)} + \text{N}_2$. With permission to reprint from Ref [57], Copyright 2015, Wiley-VCH.

Likewise, the performance is not optimized with known best catalyst. Thus, the development of ammonia decomposition at low temperature for onsite hydrogen generation needs to be more comprehensive. The most promising nitride imide composite catalysts should also be integrated with catalytic membrane reactor to investigate their effectiveness at low temperature to realize 100% conversion.

5. Summary and perspective

The ammonia decomposition reaction is an endothermic reaction whose equilibrium conversion is 99.5% at 450 °C but the fast kinetics and heat transfer limitations limit the conversion efficiency at low temperature. Hence, high temperature is required for attaining complete conversion even with different catalyst. Along with the

Table 4
Brief summary of common reactors used and developed for ammonia decomposition reaction.

Type of Reactor	Properties	Limitation	Performance
Fixed Bed Reactor	High pressure drop; difficulty in maintaining flow rates	Large temperature gradient limits extent of ammonia decomposition; Not suitable for fast catalytic reactions;	Higher the feed temperature, higher the conversion; Temperature Range 600–900 °C [162]
Microreactor	Characteristic length in the order of sub mm; Eliminates temperature gradient; Good for fast catalytic reactions	Difficult to scale up for industrial applications; also shows mass transfer limitations in some cases;	Conversion 97.0% with feed of $\text{NH}_3\text{-H}_2$ mixture; temperature 400–700 °C; L = 55 mm D = 16 mm; 10 Nml/min P = 1 bar Efficiency = 10.4% [163]
Micropost Reactor	Consists of catalyst covered pillar like structures within microchannel to reduce mass transfer limitation	Conversion depends on pore size; tradeoff required between conversion and pore size; Have not been reported yet;	Conversion: 85%; flow rate: 15 Nml/min; T = 650 °C P = 1 bar [164]
Membrane Reactor	Removal of H_2 from reaction zone enhances equilibrium conversion at low temperature; Lowers system capital and operating costs;	Use of Pd membrane reduces H_2 selectivity; Mostly reported using dilute ammonia; partial pressure of ammonia alters conversion; Sweep gas dilutes H_2	50–400 Nml/min T = 425–500 °C; P = 1–5 bar; Conversion:(55–99)% [165]
Catalytic Membrane Reactor (3D CFD Simulation)	Used metal coated sandwich membranes inside catalyst bed;	Fixed retentate pressure of 10 bar had to be maintained to ensure sufficient permeation of H_2	Conversion of 99,93% was attained at a temperature of 550 °C [166]
Catalytic Membrane Reactor (Experimental)			Conversion: 74.4%; Flow rate: 40 Nml/min T = 450 °C; P = 1–3 bar [167]

development of catalyst, development of reactor is equally essential. The precious metal catalyst, Ru/CNT, under development since 2004, is widely known to be the state of the art catalyst. Its catalytic properties have been modified using supports like graphene nanocomposite, high surface area graphite, carbon nanofibers etc to increase the dispersion of Ru and tune the particle size accordingly. The best performing Ru catalyst has been obtained by doping 12 wt.% potassium on Ru and supported on MgO and CNT. With KOH modified Ru, complete conversion is achieved at a temperature around 500 °C. As the objective is onsite H₂ generation for PEM fuel cells, use of such precious metal based catalyst will not be feasible. Transition metals like Fe, Co, Ni also show catalytic activity for ammonia decomposition, but only at relatively high temperatures (> 600 °C). Transition metal nanoparticles dispersed in an alumina matrix, CNT and carbon nanofiber recently have been shown to offer significant improvement in conversion efficiency at around 550 °C. However, they are not sufficient to give 99% conversion at 450 °C and meet the U.S. DOE specifications for onboard hydrogen storage. Nitrides and carbides of transition metals also show catalytic activity for ammonia decomposition, but as single component catalysts, they, too, fall far short of target performance.

Recently, investigation of catalytic activity of sodium amide, paved the way for testing other alkali amides as catalyst for ammonia decomposition. The mechanism of decomposition of ammonia on alkali amides has been investigated and confirmed by isotopic studies for sodium amide and lithium amide. Decomposition of ammonia on lithium amide is different from sodium amide as lithium amide transforms into lithium imide above 310 °C and forms a stable solid above that temperature as lithium imide has a high decomposition temperature of 600 °C. However, this does not ensure stability of the ammonia decomposition catalyst. Lithium imide reacts with ammonia to form lithium amide again if the partial pressure of ammonia is high; i.e. the stability is a concern for high flow rate and when pure ammonia is used; similarly, for sodium amide, its low decomposition temperature is a concern for long term stability. This would also initiate difficulty in integrating catalyst with membrane reactors as well. Some authors suggested use of U tube reactor or tank reactors for containment of amide based catalyst. However, reactors have not been optimized so far.

A new research direction for metal nitrides and imides developed when it was found that there is a synergy between these nitrides and alkali/alkaline earth amides/imides as these composites display greater activity than component nitrides and imides alone. While several nitrides have been tested for catalytic decomposition of ammonia, not many studies have been reported wherein the nitrides form a composite with the imides. The activity of MnN-Li₂NH composites is comparable to the state of the art Ru/CNT catalyst. Though it is reported to be better than the state of the art catalyst, it was not compared with the best modification of Ru catalyst. However, the nitride imide composite can be much more stable than lithium amide/imide alone if they are optimized.

Another nitride/imide composite that is reported to exhibit activity greater than its individual components is Fe₂N-Li₂NH. The ternary metal nitride of lithium and the lithium imide is also promising for low temperature ammonia decomposition provided the reaction conditions and molar ratios of the components are optimized. The role and effect of supports like CNT and carbon nanofiber on these catalysts is yet to be reported. Guo et al. [57] mentioned that with CNT, lithium imide reacts to form Li₂CN₂, and hence it may not prove to be a good catalyst.

Li₂NH is also very difficult to dissolve in most organic solvents, so conventional wetness impregnation preparations methods that are used for Ru based catalysts cannot be used for synthesis of these composite catalysts. Despite all their limitations, the TM(N)-alkali metal amide/imide composite catalysts perform comparably to the state of the art catalyst and are much more effective than other non precious metal catalyst at lower temperatures. Given the relatively short time they have been under development, these composites show tremendous

promise as future catalysts for low temperature ammonia decomposition. Electrochemical synthesis of ammonia has also attracted significant attention recently by directly reducing N₂ and H₂O using electricity that is generated renewably [168,169]. The effective nitride/imide composite ammonia decomposition catalysts may be suitable for the challenging electrochemical synthesis of ammonia as well. The optimal integration of ammonia production from renewable resources and ammonia decomposition will be crucial for fully realizing carbon-free energy technologies from ammonia.

Acknowledgments

Authors acknowledge the start-up funding from the University at Buffalo (SUNY) along with U.S. Department of Energy's Advanced Research Projects Agency-Energy (ARPA-E) program.

References

- [1] J.D. Holladay, J. Hu, D.L. King, Y. Wang, An overview of hydrogen production technologies, *Catal. Today* 139 (2009) 244–260.
- [2] L. Schlapbach, A. Zettler, Hydrogen-storage materials for mobile applications, *Nature* 414 (2001) 353–358.
- [3] Exterior Dimensions of Toyota Mirai, (2016) <http://www.mytoyotamirai.com/toyota-mirai-specifications/>.
- [4] S.W. Jorgensen, Hydrogen storage tanks for vehicles: recent progress and current status, *Curr. Opin. Solid State Mater. Sci.* 15 (2011) 39–43.
- [5] G.W. Crabtree, M.S. Dresselhaus, M.V. Buchanan, The hydrogen economy, *Phys. Today* 57 (2004) 39–44.
- [6] F. Schüth, Chemical compounds for energy storage, *Chem. Ing. Tech.* 83 (2011) 1984–1993.
- [7] J.O.M. Bockris, The hydrogen economy: its history, *Int. J. Hydrogen Energy* 38 (2013) 2579–2588.
- [8] M. Ball, M. Weeda, The hydrogen economy—vision or reality? *Int. J. Hydrogen Energy* 40 (2015) 7903–7919.
- [9] R. Lan, J.T. Irvine, S. Tao, Ammonia and related chemicals as potential indirect hydrogen storage materials, *Int. J. Hydrogen Energy* 37 (2012) 1482–1494.
- [10] M. Yadav, Q. Xu, Liquid-phase chemical hydrogen storage materials, *Energy Environ. Sci.* 5 (2012) 9698–9725.
- [11] A.F. Dalebrook, W. Gan, M. Grasemann, S. Moret, G. Laurenczy, Hydrogen storage: beyond conventional methods, *Chem. Commun.* 49 (2013) 8735–8751.
- [12] A. Klerke, C.H. Christensen, J.K. Nørskov, T. Vegge, Ammonia for hydrogen storage: challenges and opportunities, *J. Mater. Chem.* 18 (2008) 2304–2310.
- [13] R.O. Idem, N.N. Bakhshi, Production of hydrogen from methanol. Part 1. Catalyst characterization studies, *Ind. Eng. Chem. Res.* 33 (1994) 2047–2055.
- [14] R.H. Wiswall, J.J. Reilly, Hydrogen storage in metal-hydrides – comment, *Science* 186 (1974) 1158–1158.
- [15] A. Zettler, P. Sudan, P. Mauron, T. Kiyobayashi, C. Emmenegger, L. Schlapbach, Hydrogen storage in carbon nanostructures, *Int. J. Hydrogen Energy* 27 (2002) 203–212.
- [16] C.H. Christensen, R.Z. Sørensen, T. Johannessen, U.J. Quaade, K. Honkala, T.D. Elmøe, R. Køhler, J.K. Nørskov, Metal ammine complexes for hydrogen storage, *J. Mater. Chem.* 15 (2005) 4106–4108.
- [17] R.Z. Sørensen, J.S. Hummelshøj, A. Klerke, J.B. Reves, T. Vegge, J.K. Nørskov, C.H. Christensen, Indirect: reversible high-density hydrogen storage in compact metal ammine salts, *J. Am. Chem. Soc.* 130 (2008) 8660–8668.
- [18] A. Boisen, S. Dahl, J.K. Nørskov, C.H. Christensen, Why the optimal ammonia synthesis catalyst is not the optimal ammonia decomposition catalyst, *J. Catal.* 230 (2005) 309–312.
- [19] C.H. Christensen, T. Johannessen, R.Z. Sørensen, J.K. Nørskov, Towards an ammonia-mediated hydrogen economy? *Catal. Today* 111 (2006) 140–144.
- [20] C. Zamfirescu, I. Dincer, Ammonia as a green fuel and hydrogen source for vehicular applications, *Fuel Process. Technol.* 90 (2009) 729–737.
- [21] Y. Tanabe, Y. Nishibayashi, Developing more sustainable processes for ammonia synthesis, *Coord. Chem. Rev.* 257 (2013) 2551–2564.
- [22] C. Zamfirescu, I. Dincer, Using ammonia as a sustainable fuel, *J. Power Sources* 185 (2008) 459–465.
- [23] R. Metkemeijer, P. Achard, Comparison of ammonia and methanol applied indirectly in a hydrogen fuel cell, *Int. J. Hydrogen Energy* 19 (1994) 535–542.
- [24] R. Metkemeijer, P. Achard, Ammonia as a feedstock for a hydrogen fuel-cell – reformer and fuel-cell behavior, *J. Power Sources* 49 (1994) 271–282.
- [25] W.I.F. David, J.W. Makepeace, S.K. Callear, H.M.A. Hunter, J.D. Taylor, T.J. Wood, M.O. Jones, Hydrogen production from ammonia using sodium amide, *J. Am. Chem. Soc.* 136 (2014) 13082–13085.
- [26] L. Green, An ammonia energy vector for the hydrogen economy, *Int. J. Hydrogen Energy* 7 (1982) 355–359.
- [27] R. Lan, J.T.S. Irvine, S. Tao, Ammonia and related chemicals as potential indirect hydrogen storage materials, *Int. J. Hydrogen Energy* 37 (2012) 1482–1494.
- [28] R. Lan, S. Tao, Ammonia as a suitable fuel for fuel cells, *Front. Energy Res.* 2 (2014) 35.
- [29] F. Schueth, R. Palkovits, R. Schloegl, D.S. Su, Ammonia as a possible element in an

energy infrastructure: catalysts for ammonia decomposition, *Energy Environ. Sci.* 5 (2012) 6278–6289.

[30] G. Thomas¹, a.G. Parks, US Department of Energy, (2006).

[31] T. Hejze, J. Besenhard, K. Kordes, M. Cifrain, R. Aronsson, Current status of combined systems using alkaline fuel cells and ammonia as a hydrogen carrier, *J. Power Sources* 176 (2008) 490–493.

[32] C.J.H. Jacobsen, S. Dahl, B.S. Clausen, S. Bahn, A. Logadottir, J.K. Norskov, Catalyst design by interpolation in the periodic table: bimetallic ammonia synthesis catalysts, *J. Am. Chem. Soc.* 123 (2001) 8404–8405.

[33] C. Egawa, T. Nishida, S. Naito, K. Tamaru, Ammonia decomposition on (1110) and (001) surfaces of ruthenium, *J. Chem. Soc.-Faraday Trans. I* 80 (1984) 1595–1604.

[34] S.F. Yin, B.Q. Xu, S.J. Wang, C.F. Ng, C.T. Au, Magnesia–carbon nanotubes (MgO–CNTs) nanocomposite: novel support of Ru catalyst for the generation of CO_x-free hydrogen from ammonia, *Catal. Lett.* 96 (2004) 113–116.

[35] J. Chen, Z.H. Zhu, S. Wang, Q. Ma, V. Rudolph, G.Q. Lu, Effects of nitrogen doping on the structure of carbon nanotubes (CNTss) and activity of Ru/CNTs in ammonia decomposition, *Chem. Eng. J.* 156 (2010) 404–410.

[36] S.F. Yin, B.Q. Xu, W.X. Zhu, C.F. Ng, X.P. Zhou, C.T. Au, Carbon nanotubes-supported Ru catalyst for the generation of cox-free hydrogen from ammonia, *Catal. Today* 93–95 (2004) 27–38.

[37] H.S. Zeng, K. Inazu, K. Aika, The working state of the barium promoter in ammonia synthesis over an active-carbon-supported ruthenium catalyst using barium nitrate as the promoter precursor, *J. Catal.* 211 (2002) 33–41.

[38] E.P. Perman, G.A.S. Atkinson, The decomposition of ammonia by heat, *Proc. R. Soc. Lond.* 74 (1904) 110–117.

[39] J.-L. Cao, Z.-L. Yan, Q.-F. Deng, Z.-Y. Yuan, Y. Wang, G. Sun, X.-D. Wang, B. Hari, Z.-Y. Zhang, Homogeneous precipitation method preparation of modified red mud supported Ni mesoporous catalysts for ammonia decomposition, *Catal. Sci. Technol.* 4 (2014) 361–368.

[40] F. Hayashi, Y. Toda, Y. Kanie, M. Kitano, Y. Inoue, T. Yokoyama, M. Hara, H. Hosono, Ammonia decomposition by ruthenium nanoparticles loaded on inorganic electrode C12A7:e[−], *Chem. Sci.* 4 (2013) 3124–3130.

[41] Y. Marco, L. Roldán, S. Armenise, E. García-Bordejé, Support-induced oxidation state of catalytic Ru nanoparticles on carbon nanofibers that were doped with heteroatoms (O, N) for the decomposition of NH₃, *ChemCatChem* 5 (2013) 3829–3834.

[42] S.B. Simonsen, D. Chakraborty, I. Chorkendorff, S. Dahl, Alloyed Ni-Fe nanoparticles as catalysts for NH₃ decomposition, *Appl. Catal. A: Gen.* 447–448 (2012) 22–31.

[43] A. Di Carlo, L. Vecchione, Z. Del Prete, Ammonia decomposition over commercial Ru/Al₂O₃ catalyst: an experimental evaluation at different operative pressures and temperatures, *Int. J. Hydrogen Energy* 39 (2014) 808–814.

[44] J. Ji, X. Duan, G. Qian, P. Li, X. Zhou, D. Chen, W. Yuan, Fe particles on the tops of carbon nanofibers immobilized on structured carbon microfibers for ammonia decomposition, *Catal. Today* 216 (2013) 254–260.

[45] V. Tagliazucca, K. Schlichte, F. Schüth, C. Weidenthaler, Molybdenum-based catalysts for the decomposition of ammonia: in situ X-ray diffraction studies, microstructure, and catalytic properties, *J. Catal.* 305 (2013) 277–289.

[46] Z. Kowalczyk, J. Sentek, S. Jodzis, M. Muhler, O. Hinrichsen, Effect of potassium on the kinetics of ammonia synthesis and decomposition over fused iron catalyst at atmospheric pressure, *J. Catal.* 169 (1997) 407–414.

[47] W. Arabczyk, U. Narkiewicz, A new method for in situ determination of number of active sites in iron catalysts for ammonia synthesis and decomposition, *Appl. Surf. Sci.* 196 (2002) 423–428.

[48] G. Novell-Leruth, A. Valcárce, J. Pérez-Ramírez, J.M. Ricart, Ammonia dehydrogenation over platinum-group metal surfaces. Structure, stability, and reactivity of adsorbed NH_x species, *J. Phys. Chem. C* 111 (2007) 860–868.

[49] A. Amano, H. Taylor, The decomposition of ammonia on ruthenium: rhodium and palladium catalysts supported on alumina, *J. Am. Chem. Soc.* 76 (1954) 4201–4204.

[50] W. Arabczyk, J. Zamlynny, Study of the ammonia decomposition over iron catalysts, *Catal. Lett.* 60 (1999) 167–171.

[51] S. Brunauer, K.S. Love, R.G. Keenan, Adsorption of nitrogen and the mechanism of ammonia decomposition over iron catalysts, *J. Am. Chem. Soc.* 64 (1942) 751–758.

[52] J.C. Ganley, F.S. Thomas, E.G. Seebauer, R.I. Masel, A priori catalytic activity correlations: the difficult case of hydrogen production from ammonia, *Catal. Lett.* 96 (2004) 117–122.

[53] B. Lorenzut, T. Montini, C.C. Pavel, M. Comotti, F. Vizza, C. Bianchini, P. Fornasier, Embedded Ru@ZrO₂ catalysts for H₂ production by ammonia decomposition, *ChemCatChem* 2 (2010) 1096–1106.

[54] C. Liang, W. Li, Z. Wei, Q. Xin, C. Li, Catalytic decomposition of ammonia over nitrided Mo_N/ α -Al₂O₃ and nimony/ α -Al₂O₃ catalysts, *Ind. Eng. Chem. Res.* 39 (2000) 3694–3697.

[55] S.-F. Yin, B.-Q. Xu, C.-F. Ng, C.-T. Au, Nano Ru/CNTs: a highly active and stable catalyst for the generation of CO_x-free hydrogen in ammonia decomposition, *Appl. Catal. B: Environ.* 48 (2004) 237–241.

[56] S.F. Yin, B.Q. Xu, X.P. Zhou, C.T. Au, A mini-review on ammonia decomposition catalysts for on-site generation of hydrogen for fuel cell applications, *Appl. Catal. A: Gen.* 277 (2004) 1–9.

[57] J. Guo, P. Wang, G. Wu, A. Wu, D. Hu, Z. Xiong, J. Wang, P. Yu, F. Chang, Z. Chen, P. Chen, Lithium imide synergy with 3d transition-metal nitrides leading to unprecedented catalytic activities for ammonia decomposition, *Angew. Chem. Int. Ed.* 54 (2015) 2950–2954.

[58] Y.A. Alhamed, H. Zhang, Y. Kojima, A.A. Al-Zahrani, D. Hafedh, L.A. Petrov, Effect of surface functional groups attached to carbon nanotubes used as support of nickel catalysts on their structure and catalytic performance for ammonia decomposition, *Comptes Rendus De L Academie Bulgare Des Sciences* 67 (2014) 519–526.

[59] K. Okura, T. Okanishi, H. Muroyama, T. Matsui, K. Eguchi, Ammonia decomposition over nickel catalysts supported on rare-earth oxides for the on-site generation of hydrogen, *ChemCatChem* 8 (2016) 2988–2995.

[60] H. Inokawa, T. Ichikawa, H. Miyao, Catalysis of nickel nanoparticles with high thermal stability for ammonia decomposition, *Appl. Catal. A: Gen.* 491 (2015) 184–188.

[61] L. Wang, Y. Zhao, C. Liu, W. Gong, H. Guo, Plasma driven ammonia decomposition on a Fe-catalyst: eliminating surface nitrogen poisoning, *Chem. Commun.* 49 (2013) 3787–3789.

[62] X. Duan, G. Qian, X. Zhou, Z. Sui, D. Chen, W. Yuan, Tuning the size and shape of Fe nanoparticles on carbon nanofibers for catalytic ammonia decomposition, *Appl. Catal. B: Environ.* 101 (2011) 189–196.

[63] Z. Lendzion-Bielun, U. Narkiewicz, W. Arabczyk, Cobalt-based catalysts for ammonia decomposition, *Materials* 6 (2013) 2400.

[64] X. Duan, J. Ji, X. Yan, G. Qian, D. Chen, X. Zhou, Understanding Co-Mo catalyzed ammonia decomposition: influence of calcination atmosphere and identification of active phase, *ChemCatChem* 8 (2016) 938–945.

[65] M. Winter, R.J. Brodd, What are batteries, fuel cells, and supercapacitors? *Chem. Rev.* 104 (2004) 4245–4270.

[66] S.F. Yin, Q.H. Zhang, B.Q. Xu, W.X. Zhu, C.F. Ng, C.T. Au, Investigation on the catalysis of CO_x-free hydrogen generation from ammonia, *J. Catal.* 224 (2004) 384–396.

[67] T.E. Bell, L. Torrente-Murciano, H₂ production via ammonia decomposition using non-noble metal catalysts: a review, *Top. Catal.* 59 (2016) 1438–1457.

[68] M.C.J. Bradford, P.E. Fanning, M.A. Vannice, Kinetics of NH₃ decomposition over well dispersed Ru, *J. Catal.* 172 (1997) 479–484.

[69] M.E.E. Abashar, Y.S. Al-Sughair, I.S. Al-Mutaz, Investigation of low temperature decomposition of ammonia using spatially patterned catalytic membrane reactors, *Appl. Catal. A: Gen.* 236 (2002) 35–53.

[70] V. Alaghari, S. Palanki, K.N. West, Analysis of ammonia decomposition reactor to generate hydrogen for fuel cell applications, *J. Power Sources* 195 (2010) 829–833.

[71] S. Chiuta, R.C. Everson, H. Neomagus, P. van der Gryp, D.G. Bessarabov, Reactor technology options for distributed hydrogen generation via ammonia decomposition: a review, *Int. J. Hydrogen Energy* 38 (2013) 14968–14991.

[72] J.P. Collins, J.D. Way, Catalytic decomposition of ammonia in a membrane reactor, *J. Membr. Sci.* 96 (1994) 255–274.

[73] L. Meng, T. Tsuru, Hydrogen production from energy carriers by silica-based catalytic membrane reactors, *Catal. Today* 268 (2016) 3–11.

[74] C. Plana, S. Armenise, A. Monzon, E. Garcia-Bordeje, Process optimisation of in situ H₂ generation from ammonia using Ni on alumina coated cordierite monoliths, *Top. Catal.* 54 (2011) 914–921.

[75] E. Rizzuto, P. Palange, Z. Del Prete, Characterization of an ammonia decomposition process by means of a multifunctional catalytic membrane reactor, *Int. J. Hydrogen Energy* 39 (2014) 11403–11410.

[76] F.R. Garcia-Garcia, A. Guerrero-Ruiz, I. Rodriguez-Ramos, A. Goguet, S.O. Shekhtman, C. Hardacre, Tap studies of ammonia decomposition over Ru and Ir catalysts, *Phys. Chem. Chem. Phys.* 13 (2011) 12892–12899.

[77] F.R. Garcia-Garcia, A. Guerrero-Ruiz, I. Rodriguez-Ramos, Role of B5-type sites in Ru catalysts used for the NH₃ decomposition reaction, *Top. Catal.* 52 (2009) 758–764.

[78] H. Mortensen, L. Diekhöner, A. Baurichter, E. Jensen, A. Luntz, Dynamics of ammonia decomposition on Ru (0001), *J. Chem. Phys.* 113 (2000) 6882–6887.

[79] X. Duan, J. Ji, G. Qian, C. Fan, Y. Zhu, X. Zhou, D. Chen, W. Yuan, Ammonia decomposition on Fe(110): Co(111) and Ni(111) surfaces: a density functional theory study, *J. Mol. Catal. A: Chem.* 357 (2012) 81–86.

[80] W. Tsai, W.H. Weinberg, Steady-state decomposition of ammonia on the ruthenium(001) surface, *J. Phys. Chem.* 91 (1987) 5302–5307.

[81] W. Pyrz, R. Vijay, J. Binz, J. Lauterbach, D.J. Buttrey, Characterization of K-promoted Ru catalysts for ammonia decomposition discovered using high-throughput experimentation, *Top. Catal.* 50 (2008) 180–191.

[82] A.S. Chellappa, C.M. Fischer, W.J. Thomson, Ammonia decomposition kinetics over Ni-Pt/Al₂O₃ for pem fuel cell applications, *Appl. Catal. A: Gen.* 227 (2002) 231–240.

[83] K. Tamaru, A. new general mechanism of ammonia synthesis and decomposition on transition metals, *Acc. Chem. Res.* 21 (1988) 88–94.

[84] G. Papapolymerou, V. Bontozoglou, Decomposition of NH₃ on Pd and Ir comparison with Pt and Rh, *J. Mol. Catal. A: Chem.* 120 (1997) 165–171.

[85] T.V. Choudhary, C. Sivadinarayana, D.W. Goodman, Catalytic ammonia decomposition: cox-free hydrogen production for fuel cell applications, *Catal. Lett.* 72 (2001) 197–201.

[86] R.I. Levy, B.M. Rifkind, Diagnosis and management of hyperlipoproteinemia in infants and children, *Am. J. Cardiol.* 31 (1973) 547–556.

[87] M. Boudart, S.T. Oyama, L. Leclercq, Molybdenum carbide, oxycarbide and nitride as catalysts in the activation of Co, N-N, C-C and H-H bonds, in: T. Seiyama, K. Tanabe (Eds.), *Studies in Surface Science and Catalysis*, Elsevier, 1981, pp. 578–590.

[88] R.B. Levy, M. Boudart, Platinum-like behavior of tungsten carbide in surface catalysis, *Science* 181 (1973) 547–549.

[89] W. Zheng, T.P. Cotter, P. Kaghazchi, T. Jacob, B. Frank, K. Schlichte, W. Zhang, D.S. Su, F. Schüth, R. Schlögl, Experimental and theoretical investigation of molybdenum carbide and nitride as catalysts for ammonia decomposition, *J. Am. Chem. Soc.* 135 (2013) 3458–3464.

[90] J.-G. Choi, Ammonia decomposition over vanadium carbide catalysts, *J. Catal.* 182 (1999) 104–116.

[91] S.T. Oyama, Kinetics of ammonia decomposition on vanadium nitride, *J. Catal.* 133 (1992) 358–369.

[92] W.J. McGill, F. Sebba, The kinetics of ammonia decomposition over vanadium nitride, *J. Catal.* 2 (1963) 104–108.

[93] L. Volpe, M. Boudart, Compounds of molybdenum and tungsten with high specific surface area, *J. Solid State Chem.* 59 (1985) 332–347.

[94] L. Volpe, M. Boudart, Compounds of molybdenum and tungsten with high specific surface area, *J. Solid State Chem.* 59 (1985) 348.

[95] H. Soerijanto, C. Rödel, U. Wild, M. Lerch, R. Schomäcker, R. Schlägl, T. Ressler, The impact of nitrogen mobility on the activity of zirconium oxynitride catalysts for ammonia decomposition, *J. Catal.* 250 (2007) 19–24.

[96] J. Wendel, M. Lerch, W. Laqua, Novel zirconia-based superionic conductors: the electrical conductivity of Y-Zr-O-N materials, *J. Solid State Chem.* 142 (1999) 163–167.

[97] M. Kilo, M.A. Taylor, C. Argirusis, G. Borchardt, M. Lerch, O. Kaitasov, B. Lesage, Nitrogen diffusion in nitrogen-doped yttria stabilised zirconia, *Phys. Chem. Chem. Phys.* 6 (2004) 3645–3649.

[98] A.W. Titherley, Xlv.-sodium, potassium, and lithium amides, *J. Chem. Soc. Trans.* 65 (1894) 504–522.

[99] T.J. Wood, J.W. Makepeace, H.M.A. Hunter, M.O. Jones, W.I.F. David, Isotopic studies of the ammonia decomposition reaction mediated by sodium amide, *Phys. Chem. Chem. Phys.* 17 (2015) 22999–23006.

[100] P. Chen, Z. Xiong, G. Wu, Y. Liu, J. Hu, W. Luo, Metal-N-H systems for the hydrogen storage, *Scr. Mater.* 56 (2007) 817–822.

[101] P. Chen, Z.T. Xiong, J.Z. Luo, J.Y. Lin, K.L. Tan, Interaction of hydrogen with metal nitrides and imides, *Nature* 420 (2002) 302–304.

[102] E. Hazrati, G. Brocks, B. Buurman, R.A. de Groot, G.A. de Wijs, Intrinsic defects and dopants in LiNH₂: a first-principles study, *Phys. Chem. Chem. Phys.* 13 (2011) 6043–6052.

[103] S. Hino, T. Ichikawa, Y. Kojima, Thermodynamic properties of metal amides determined by ammonia pressure-composition isotherms, *J. Chem. Thermodyn.* 42 (2010) 140–143.

[104] T. Ichikawa, N. Hanada, S. Isobe, H.Y. Leng, H. Fujii, Mechanism of novel reaction from LiNH₂ and lih to Li₂NH and H₂ as a promising hydrogen storage system, *J. Phys. Chem. B* 108 (2004) 7887–7892.

[105] G. Miceli, C.S. Cucinotta, M. Bernasconi, M. Parrinello, First principles study of the LiNH₂/Li₂NH transformation, *J. Phys. Chem. C* 114 (2010) 15174–15183.

[106] J.W. Makepeace, T.J. Wood, H.M.A. Hunter, M.O. Jones, W.I.F. David, Ammonia decomposition catalysis using non-stoichiometric lithium imide, *Chem. Sci.* 6 (2015) 3805–3815.

[107] I.E. Gabis, A.P. Voit, E.A. Evard, Y.V. Zaika, I.A. Chernov, V.A. Yartys, Kinetics of hydrogen desorption from the powders of metal hydrides, *J. Alloys Compd.* 404–406 (2005) 312–316.

[108] G. Mulas, L. Schiffini, G. Tanda, G. Cocco, Hydriding kinetics and process parameters in reactive milling, *J. Alloys Compd.* 404–406 (2005) 343–346.

[109] E. Orgaz, A. Membrillo, R. Castañeda, A. Aburto, Electronic structure of ternary hydrides based on light elements, *J. Alloys Compd.* 404–406 (2005) 176–180.

[110] M. Yoshino, K. Komiya, Y. Takahashi, Y. Shinzato, H. Yukawa, M. Morinaga, Nature of the chemical bond in complex hydrides, NaAlH₄, LiAlH₄ and LiNH₂, *J. Alloys Compd.* 404–406 (2005) 185–190.

[111] G.P. Meissner, F.E. Pinkerton, M.S. Meyer, M.P. Balogh, M.D. Kundrat, Study of the lithium–nitrogen–hydrogen system, *J. Alloys Compd.* 404–406 (2005) 24–26.

[112] K. Miwa, N. Ohba, S.-i. Towata, Y. Nakamori, S.-i. Orimo, First-principles study on lithium amide for hydrogen storage, *Phys. Rev. B* 71 (2005) 195109.

[113] J. Zhang, Y.H. Hu, Intermediate species and kinetics of lithium imide decomposition, *Int. J. Hydrogen Energy* 37 (2012) 10467–10472.

[114] T.J. Wood, J.W. Makepeace, W.I.F. David, Isotopic studies of the ammonia decomposition reaction using lithium imide catalyst, *Phys. Chem. Chem. Phys.* (2017).

[115] J.W. Makepeace, H.M.A. Hunter, T.J. Wood, R.I. Smith, C.A. Murray, W.I.F. David, Ammonia decomposition catalysis using lithium-calcium imide, *Faraday Discuss.* 188 (2016) 525–544.

[116] S.J. Wang, S.F. Yin, L. Li, B.Q. Xu, C.F. Ng, C.T. Au, Investigation on modification of Ru/CNTs catalyst for the generation of cox-free hydrogen from ammonia, *Appl. Catal. B: Environ.* 52 (2004) 287–299.

[117] R.Z. Sorensen, A. Klerke, U. Quaade, S. Jensen, O. Hansen, C.H. Christensen, Promoted ru on high-surface area graphite for efficient miniaturized production of hydrogen from ammonia, *Catal. Lett.* 112 (2006) 77–81.

[118] G. Li, M. Kanezashi, T. Tsuru, Catalytic ammonia decomposition over high-performance ru/graphene nanocomposites for efficient cox-free hydrogen production, *Catalysts* 7 (2017) 23.

[119] A.M. Karim, V. Prasad, G. Mpourmpakis, W.W. Lonergan, A.I. Frenkel, J.G. Chen, D.G. Vlachos, Correlating particle size and shape of supported Ru/γ-Al₂O₃ catalysts with nh3 decomposition activity, *J. Am. Chem. Soc.* 131 (2009) 12230–12239.

[120] L. Wang, J.L. Chen, L. Ge, V. Rudolph, Z.H. Zhu, Difference in the cooperative interaction between carbon nanotubes and Ru particles loaded on their internal/external surface, *RSC Adv.* 3 (2013) 12641–12647.

[121] W. Zheng, A. Thomas, R. Schlägl, R. Schomäcker, K. Rademann, T. Ressler, Technische Universität Berlin, (2011).

[122] W. Raróg-Pilecka, E. Miśkiewicz, D. Szmigiel, Z. Kowalczyk, Structure sensitivity of ammonia synthesis over promoted ruthenium catalysts supported on graphitised carbon, *J. Catal.* 231 (2005) 11–19.

[123] C.J.H. Jacobsen, S. Dahl, P.L. Hansen, E. Törnqvist, L. Jensen, H. Topsøe, D.V. Prip, P.B. Møenshaug, I. Chorkendorff, Structure sensitivity of supported ruthenium catalysts for ammonia synthesis, *J. Mol. Catal. A: Chem.* 163 (2000) 19–26.

[124] F.R. García-García, J. Álvarez-Rodríguez, I. Rodríguez-Ramos, A. Guerrero-Ruiz, The use of carbon nanotubes with and without nitrogen doping as support for ruthenium catalysts in the ammonia decomposition reaction, *Carbon* 48 (2010) 267–276.

[125] W. Raróg-Pilecka, D. Szmigiel, Z. Kowalczyk, S. Jodzis, J. Zieliński, Ammonia decomposition over the carbon-based ruthenium catalyst promoted with barium or cesium, *J. Catal.* 218 (2003) 465–469.

[126] Z. Kowalczyk, M. Krukowski, W. Rarög-Pilecka, D. Szmigiel, J. Zieliński, Carbon-based ruthenium catalyst for ammonia synthesis – role of the barium and caesium promoters and carbon support, *Appl. Catal. A-Gen.* 248 (2003) 67–73.

[127] A.K. Hill, L. Torrente-Murciano, In-situ H₂ production via low temperature decomposition of ammonia: insights into the role of cesium as a promoter, *Int. J. Hydrogen Energy* 39 (2014) 7646–7654.

[128] P. Yu, J. Guo, L. Liu, P. Wang, F. Chang, H. Wang, X. Ju, P. Chen, Effects of alkaline earth metal amides on ru in catalytic ammonia decomposition, *J. Phys. Chem. C* 120 (2016) 2822–2828.

[129] R. Pelka, W. Arabczyk, Influence of chemical composition of nanocrystalline iron's surface on the rates of two parallel reactions: nitriding and catalytic decomposition of ammonia, *Chem. Pap.* 66 (2012) 18–25.

[130] A. Jedynak, Z. Kowalczyk, D. Szmigiel, W. Rarög, J. Zieliński, Ammonia decomposition over the carbon-based iron catalyst promoted with potassium, *Appl. Catal. A: Gen.* 237 (2002) 223–226.

[131] G. Ertl, M. Huber, Mechanism and kinetics of ammonia decomposition on iron, *J. Catal.* 61 (1980) 537–539.

[132] D.G. Löffler, L.D. Schmidt, Kinetics of NH₃ decomposition on iron at high temperatures, *J. Catal.* 44 (1976) 244–258.

[133] K. Kielbasa, R. Pelka, W. Arabczyk, Studies of the kinetics of ammonia decomposition on promoted nanocrystalline iron using gas phases of different nitriding degree, *J. Phys. Chem. A* 114 (2010) 4531–4534.

[134] H. Tüysüz, F. Schüth, L. Zhi, K. Müllen, M. Comotti, Ammonia decomposition over iron phthalocyanine-based materials, *ChemCatChem* 7 (2015) 1453–1459.

[135] J. Zhang, M. Comotti, F. Schuth, R. Schlogl, D.S. Su, Commercial Fe- or Co-containing carbon nanotubes as catalysts for NH₃ decomposition, *Chem. Commun.* (2007) 1916–1918.

[136] J. Zhang, J.O. Muller, W.Q. Zheng, D. Wang, D.S. Su, R. Schlogl, Individual Fe-Co alloy nanoparticles on carbon nanotubes: structural and catalytic properties, *Nano Lett.* 8 (2008) 2738–2743.

[137] J. Zhang, H. Xu, W. Li, Kinetic study of NH₃ decomposition over ni nanoparticles: the role of La promoter, structure sensitivity and compensation effect, *Appl. Catal. A: Gen.* 296 (2005) 257–267.

[138] M. Grunze, M. Golze, R.K. Driscoll, P.A. Dowben, Ammonia adsorption and decomposition on a Ni(110) surface, *J. Vac. Sci. Technol.* 18 (1981) 611–615.

[139] C.W. Seabury, T.N. Rhodin, R.J. Purtell, R.P. Merrill, Chemisorption and reaction of NH₃ on Ni(111), *Surf. Sci.* 93 (1980) 117–126.

[140] Y. Liu, H. Wang, J. Li, Y. Lu, H. Wu, Q. Xue, L. Chen, Monolithic microfibrous nickel catalyst co-modified with ceria and alumina for miniature hydrogen production via ammonia decomposition, *Appl. Catal. A: Gen.* 328 (2007) 77–82.

[141] H. Zhang, Y.A. Alhamed, Y. Kojima, A.A. Al-Zahrani, H. Miyaoka, L.A. Petrov, Structure and catalytic properties of Ni/MWCNTs and Ni/AC catalysts for hydrogen production via ammonia decomposition, *Int. J. Hydrogen Energy* 39 (2014) 277–287.

[142] H. Zhang, Y.A. Alhamed, Y. Kojima, A.A. Al-Zahrani, L.A. Petrov, Cobalt supported on carbon nanotubes. An efficient catalyst for ammonia decomposition, *Comptes rendus de l'Académie bulgare des Sciences* 66 (2013).

[143] H. Zhang, Y.A. Alhamed, W. Chu, Z. Ye, A. AlZahrani, L. Petrov, Controlling co-support interaction in Co/MWCNTs catalysts and catalytic performance for hydrogen production via NH₃ decomposition, *Appl. Catal. A: Gen.* 464–465 (2013) 156–164.

[144] L. Czekajlo, Z. Lendzion-Bielun, Effect of preparation conditions and promoters on the structure and activity of the ammonia decomposition reaction catalyst based on nanocrystalline cobalt, *Chem. Eng. J.* 289 (2016) 254–260.

[145] Y.-Q. Gu, Z. Jin, H. Zhang, R.-J. Xu, M.-J. Zheng, Y.-M. Guo, Q.-S. Song, C.-J. Jia, Transition metal nanoparticles dispersed in an alumina matrix as active and stable catalysts for cox-free hydrogen production from ammonia, *J. Mater. Chem. A* 3 (2015) 17172–17180.

[146] C.J.H. Jacobsen, S. Dahl, A. Boisen, B.S. Clausen, H. Topsøe, A. Logadottir, J.K. Norskov, Optimal catalyst curves: connecting density functional theory calculations with industrial reactor design and catalyst selection, *J. Catal.* 205 (2002) 382–387.

[147] E. García-Bordejé, S. Armenise, L. Roldán, Toward practical application of H₂ generation from ammonia decomposition guided by rational catalyst design, *Catal. Rev.* 56 (2014) 220–237.

[148] F. Bozso, G. Ertl, M. Grunze, M. Weiss, Interaction of nitrogen with iron surfaces, *J. Catal.* 49 (1977) 18–41.

[149] J.P. Guo, Z. Chen, A.A. Wu, F. Chang, P.K. Wang, D.Q. Hu, G.T. Wu, Z.T. Xiong, P. Yu, P. Chen, Electronic promoter or reacting species? The role of LiNH₂ on ru in catalyzing nh3 decomposition, *Chem. Commun.* 51 (2015) 15161–15164.

[150] J. Guo, F. Chang, P. Wang, D. Hu, P. Yu, G. Wu, Z. Xiong, P. Chen, Highly active mn–li2nh composite catalyst for producing cox-free hydrogen, *ACS Catal.* 5 (2015) 2708–2713.

[151] P. Yu, J. Guo, L. Liu, P. Wang, G. Wu, F. Chang, P. Chen, Ammonia decomposition with manganese nitride–calcium imide composites as efficient catalysts, *ChemSusChem* 9 (2016) 364–369.

[152] Z. Jiang, P. Qin, T. Fang, Theoretical study of NH₃ decomposition on pd-cu (111) and cu-pd (111) surfaces: a comparison with clean pd (111) and cu (111), *Appl. Surf. Sci.* 371 (2016) 337–342.

[153] B. Lorenzut, T. Montini, M. Bevilacqua, P. Fornasiero, Femo-based catalysts for H₂ production by NH₃ decomposition, *Appl. Catal. B: Environ.* 125 (2012) 409–417.

[154] S. Podila, S.F. Zaman, H. Driss, Y.A. Alhamed, A.A. Al-Zahrani, L.A. Petrov, Hydrogen production by ammonia decomposition using high surface area Mo₂N and Co₂Mo₃N catalysts, *Catal. Sci. Technol.* 6 (2016) 1496–1506.

[155] D.V. Leybo, A.N. Baiguzhina, D.S. Muratov, D.I. Arkhipov, E.A. Kolesnikov, V.V. Levina, N.I. Kosova, D.V. Kuznetsov, Effects of composition and production route on structure and catalytic activity for ammonia decomposition reaction of ternary Ni–Mo nitride catalysts, *Int. J. Hydrogen Energy* 41 (2016) 3854–3860.

[156] P.L. Bramwell, S. Lentink, P. Ngene, P.E. de Jongh, Effect of pore confinement of LiNH₂ on ammonia decomposition catalysis and the storage of hydrogen and ammonia, *J. Phys. Chem. C* 120 (2016) 27212–27220.

[157] D.H. Gregory, Lithium nitrides imides and amides as lightweight, reversible hydrogen stores, *J. Mater. Chem.* 18 (2008) 2321–2330.

[158] V. Tagliazucca, M. Leoni, C. Weidenthaler, Crystal structure and microstructural changes of molybdenum nitrides traced during catalytic reaction by in situ x-ray diffraction studies, *Phys. Chem. Chem. Phys.* 16 (2014) 6182–6188.

[159] S. Hirabayashi, M. Ichihashi, Adsorption and dehydrogenation of ammonia on vanadium and niobium nitride cluster cations, *Int. J. Mass Spectrom.* 407 (2016) 86–91.

[160] S. Chiuta, R.C. Everson, H.W.J.P. Neomagus, P. van der Gryp, D.G. Bessarabov, Reactor technology options for distributed hydrogen generation via ammonia decomposition: a review, *Int. J. Hydrogen Energy* 38 (2013) 14968–14991.

[161] S. Satyapal, J. Petrovic, C. Read, G. Thomas, G. Ordaz, The u.S. Department of energy's national hydrogen storage project: progress towards meeting hydrogen-powered vehicle requirements, *Catal. Today* 120 (2007) 246–256.

[162] M.E.E. Abashar, Ultra-clean hydrogen production by ammonia decomposition, *J. King Saud Univ. – Eng. Sci.* (2016), <http://dx.doi.org/10.1016/j.jksues.2016.01.002> [in press].

[163] J.H. Kim, D.H. Um, O.C. Kwon, Hydrogen production from burning and reforming of ammonia in a microreforming system, *Energy Convers. Manage.* 56 (2012) 184–191.

[164] J.C. Ganley, E.G. Seebauer, R.I. Masel, Porous anodic alumina microreactors for production of hydrogen from ammonia, *AIChE J.* 50 (2004) 829–834.

[165] J. Zhang, H. Xu, W. Li, High-purity Co_x-free H₂ generation from NH₃ via the ultra permeable and highly selective pd membranes, *J. Membr. Sci.* 277 (2006) 85–93.

[166] A. Di Carlo, A. Dell'Era, Z. Del Prete, 3d simulation of hydrogen production by ammonia decomposition in a catalytic membrane reactor, *Int. J. Hydrogen Energy* 36 (2011) 11815–11824.

[167] G. Li, M. Kanezashi, T. Tsuru, Highly enhanced ammonia decomposition in a bimodal catalytic membrane reactor for Co_x-free hydrogen production, *Catal. Commun.* 15 (2011) 60–63.

[168] C.J. Pickett, J. Talarmin, Electrosynthesis of ammonia, *Nature* 317 (1985) 652–653.

[169] R. Michalsky, P.H. Pfromm, A. Steinfeld, Rational design of metal nitride redox materials for solar-driven ammonia synthesis, *Interface Focus* 5 (2015) 10.